

1 **Assessing Climate Change-Induced Flood Risk in the**
2 **Conasauga River Watershed: An Application of Ensemble**
3 **Hydrodynamic Inundation Modeling**

4
5 Tigstu T. Dullo¹, [George K. Darkwah](#)¹, Sudershan Gangrade^{2,3}, Mario Morales-
6 Hernández^{3,4}, Md Bulbul Sharif⁵, Alfred J. Kalyanapu^{1,*}, Shih-Chieh Kao^{2,3}, Sheikh
7 Ghafoor⁵, and Moetasim Ashfaq^{3,4}
8
9

10 ¹ Department of Civil and Environmental Engineering, Tennessee Technological
11 University, Cookeville, TN 38505, USA

12 ² Environmental Sciences Division, Oak Ridge National Laboratory, Oak Ridge, TN
13 37831, USA

14 ³ Climate Change Science Institute, Oak Ridge National Laboratory, Oak Ridge, TN
15 37831, USA

16 ⁴ Computational Sciences and Engineering Division, Oak Ridge National Laboratory,
17 Oak Ridge, TN 37831, USA

18 ⁵ Department of Computer Science, Tennessee Technological University, Cookeville, TN
19 38505, USA
20
21
22
23
24
25
26
27
28
29

30 *Corresponding Author
31 Alfred J. Kalyanapu, PhD
32 1020 Stadium Drive, P O Box 5015
33 Cookeville, TN 38505
34 Telephone: 931-372-3561
35 Email Address: akalyanapu@tntech.edu
36
37

38 Notice: This manuscript has been authored by UT-Battelle, LLC, under contract DE-AC05-
39 00OR22725 with the US Department of Energy (DOE). The US government retains and the
40 publisher, by accepting the article for publication, acknowledges that the US government retains a
41 nonexclusive, paid-up, irrevocable, worldwide license to publish or reproduce the published form
42 of this manuscript, or allow others to do so, for US government purposes. DOE will provide
43 public access to these results of federally sponsored research in accordance with the DOE Public
44 Access Plan (<http://energy.gov/downloads/doe-public-access-plan>).
45

46 **Abstract**

47 This study evaluates the impact of potential future climate change on flood regimes,
48 floodplain protection, and electricity infrastructures across the Conasauga River
49 Watershed in the southeastern United States through ensemble hydrodynamic inundation
50 modeling. The ensemble streamflow scenarios were simulated by the Distributed
51 Hydrology Soil Vegetation Model (DHSVM) driven by (1) 1981–2012 Daymet
52 meteorological observations, and (2) eleven sets of downscaled global climate models
53 (GCMs) during the 1966–2005 historical and 2011–2050 future periods. Surface
54 inundation was simulated using a GPU-accelerated Two-dimensional Runoff Inundation
55 Toolkit for Operational Needs (TRITON) hydrodynamic model. Nine out of the eleven
56 GCMs exhibit an increase in the mean ensemble flood inundation areas. Moreover, at the
57 1% annual exceedance probability level, the flood inundation frequency curves indicate a
58 ~16 km² increase in floodplain area. The assessment also shows that even after flood-
59 proofing, four of the substations could still be affected in the projected future period. The
60 increase in floodplain area and substation vulnerability highlights the need to account for
61 climate change in floodplain management. Overall, this study provides a proof-of-
62 concept demonstration of how the computationally intensive hydrodynamic inundation
63 modeling can be used to enhance flood frequency maps and vulnerability assessment
64 under the changing climatic conditions.

65

66 **Keywords:** Flood simulation; Climate change; Critical electricity infrastructure;
67 Floodplain protection standards.

68 **1. Introduction**

69 Floods are costly disasters that affect more people than any other natural hazard
70 around the world (UNISDR, 2015). Major factors that can exacerbate flood damage
71 include population growth, urbanization, and climate change (Birhanu et al., 2016;
72 Winsemius et al., 2016; Alfieri et al., 2017; Alfieri et al., 2018; Kefi et al., 2018). Recent
73 observations exhibit an increase in the frequency and the intensity of extreme
74 precipitation events (Pachauri and Meyer, 2014), which have strengthened the magnitude
75 and frequency of flooding (Milly et al., 2002; Langerwisch et al., 2013; Alfieri et al.,
76 2015a; Alfieri et al., 2018; Mora et al., 2018). As a result, the damage and cost of
77 flooding have substantially increased across the United States (US) (Pielke Jr. and
78 Downton, 2000; Pielke Jr. et al., 2002; Ntelekos et al., 2010; Wing et al., 2018) and the
79 rest of the world (Hirabayashi et al., 2013; Arnell and Gosling, 2014; Alfieri et al.,
80 2015b; Alfieri et al., 2017; Kefi et al., 2018).

81 Since 1968, the National Flood Insurance Program (NFIP), administered by the
82 Federal Emergency Management Agency (FEMA), has implemented floodplain
83 regulation standards in the US to mitigate the escalating flood losses (FEMA, 2002). For
84 communities participating in the NFIP, flood insurance is required for structures located
85 within the 1% annual exceedance probability (AEP) flood zone (i.e., areas with
86 probability of flooding $\geq 1\%$ in any given year; FEMA, 2002). However, existing
87 floodplain protection standards have proven to be inadequate (Galloway et al., 2006;
88 Ntelekos et al., 2010; Tan, 2013; Blessing et al., 2017; HCFCD, 2018), and climate
89 change can likely exacerbate these issues (Olsen, 2006; Ntelekos et al., 2010; Kollat et
90 al., 2012; AECOM, 2013; Wobus et al., 2017; Nyaupane et al., 2018; Pralle, 2019). For

91 instance, the streamflow AEP thresholds and synthetic hydrographs used to simulate the
92 flood zones were derived purely based on historic observations that may underestimate
93 the intensified hydrologic extremes in the projected future climatic conditions. Although
94 the possible change of future streamflow AEP thresholds may be evaluated by an
95 ensemble of hydrologic model outputs driven by multiple downscaled and bias-corrected
96 climate models (e.g., Wobus et al., 2017), the extension from maximum streamflow to
97 maximum flood zone is not trivial, and cannot be explicitly addressed through the
98 conventional deterministic inundation modeling approach.

99 The increases in the magnitude and frequency of flooding, in addition to the
100 inadequacy of floodplain measures and the high costs of hardening (Wilbanks et al.,
101 2008; Farber-DeAnda et al., 2010; Gilstrap et al., 2015), have put electricity
102 infrastructures at risk (Zamuda et al., 2015; Zamuda and Lippert, 2016; Cronin et al.,
103 2018; Forzieri et al., 2018; Mikellidou et al., 2018; Allen-Dumas et al., 2019). In
104 particular, electricity infrastructures which lie in areas vulnerable to flooding can
105 experience floodwater damages that may lead to changes in their energy production and
106 consumption (Chandramowli and Felder, 2014; Ciscar and Dowling, 2014; Bollinger and
107 Dijkema, 2016; Gangrade et al., 2019). For instance, flooding can rust metals, destroy
108 insulation, and damage interruption capacity (Farber-DeAnda et al., 2010; Vale, 2014;
109 NERC, 2018; Bragatto et al., 2019). It is estimated that nearly 300 energy facilities are
110 located on low-lying lands vulnerable to sea-level rise and flooding in the lower 48 US
111 states, (Strauss and Ziemlinski, 2012).

112 Several studies have assessed the vulnerability of electricity infrastructures to
113 flooding (Reed et al., 2009; Winkler et al., 2010; Bollinger and Dijkema, 2016; Fu et al.,

114 2017; Pant et al., 2017; Bragatto et al., 2019; Gangrade et al., 2019). [For highly sensitive](#)
115 [water infrastructures such as dams \(McCuen, 2005\), Gangrade et al. \(2019\) showed that](#)
116 [the surface inundation associated with probable maximum flood \(PMF\) is generally](#)
117 [projected to increase in future climate conditions. However, given the extremely large](#)
118 [magnitude of PMF \(AEP < 10⁻⁴ %\), the findings cannot be directly associated with more](#)
119 [frequent and moderate flood events \(i.e., AEP around 1–0.2%\) that are the main focus of](#)
120 [many engineering applications.](#) Although some of these studies focused on evaluating the
121 resilience of electricity infrastructures against flood hazard and/or climate change, only a
122 few of them evaluated site-specific inundation risk and quantified impacts of climate
123 change-induced flooding on electricity infrastructures under different future climate
124 scenarios. Again, one main challenge is associated with the high computational costs to
125 effectively transform ensemble streamflow projections into ensemble surface inundation
126 projections through hydrodynamic models. With the enhanced inundation models and
127 high-performance computing (HPC) capabilities (Morales-Hernández et al., 2020a), this
128 challenge can be gradually overcome for more spatially explicit flood vulnerability
129 assessment.

130 The objective of this study is to demonstrate the applicability of a computationally
131 intensive ensemble inundation modeling approach to better understand how climate
132 change may affect flood regimes, floodplain regulation standards, and the vulnerability of
133 existing infrastructures. [Extending from the framework developed by Gangrade et al.](#)
134 [\(2019\) for PMF-scale events \(AEP < 10⁻⁴ %\) based on one selected climate model](#)
135 [\(CCSM4\), we focus on more frequent extreme streamflow events \(i.e., AEP around 1–](#)
136 [0.2%\) which requires different modeling strategies based on multiple downscaled climate](#)

137 [models](#). The unique aspects of this study are the application of an integrated climate-
138 hydrologic-hydraulic modeling framework for:

139 (1) Evaluating the changes in flood regime using high-resolution ensemble flood
140 inundation maps. The ensemble-based approach is able to incorporate the large
141 hydrologic interannual variability and model uncertainty that cannot be captured
142 through the conventional deterministic flood map.

143 (2) Enabling direct frequency analysis of ensemble flood inundation maps that
144 correspond to historic and projected future climate conditions. This approach
145 provides an alternative floodplain delineation technique to the conventional
146 approach, in which a single deterministic design flood value is used to develop a
147 flood map with a given exceedance probability.

148 (3) Evaluating the vulnerability of electricity infrastructures to climate change-
149 induced flooding and assessing the adequacy of existing flood protection
150 measures using ensemble flood inundation. This information will help floodplain
151 managers to identify the most vulnerable infrastructures and recommend suitable
152 adaptation measures.

153 The following technique was adopted in this study. First, we generated streamflow
154 projection by utilizing an ensemble of simulated streamflow hydrographs driven by both
155 historical observations and downscaled climate projections (Gangrade et al., 2020) as
156 inputs for hydrodynamic inundation modeling as presented in section 2.2. Then, we set
157 up and calibrated a 2D hydrodynamic inundation model, Two-dimensional Runoff
158 Inundation Toolkit for Operational Needs (TRITON; Morales-Hernández et al.,
159 ~~2020~~[2021](#)), in our study area which is presented in section 2.3. For inundation

160 modeling, sensitivity analyses were conducted on three selected parameters to quantify
161 and compare their respective influences on modeled flood depths and extents. The
162 performance of TRITON was then evaluated by comparing a simulated 1% AEP flood
163 map with the reference 1% AEP flood map from the Federal Emergency Management
164 Agency (FEMA). Finally, as presented in sections 2.4 and 2.5, ensemble inundation
165 modeling was performed to develop flood inundation frequency curves and maps, and to
166 assess the vulnerability of electricity infrastructures under a changing climate,
167 respectively.

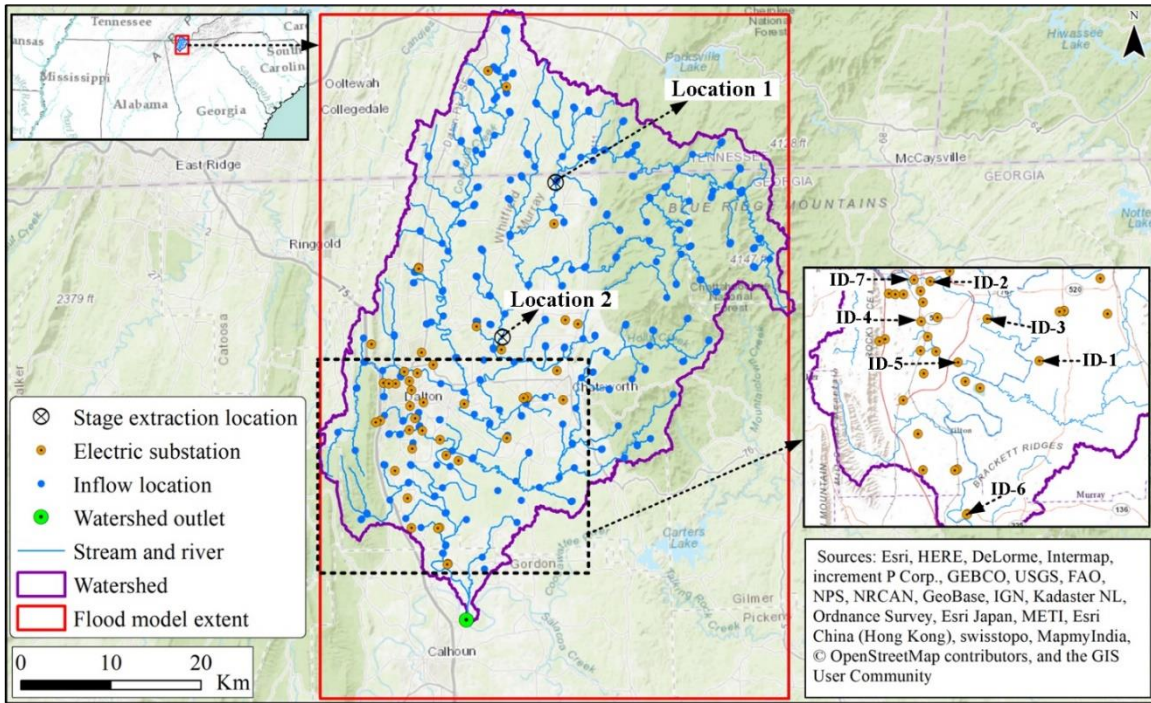
168 The article is organized as follows: the data and methods are discussed in Section 2;
169 Section 3 presents the result and discussion; and the summary is presented in Section 4.

170 **2. Data and Methods**

171 **2.1. Study Area**

172 Our study area is the Conasauga River Watershed (CRW) located in southeastern
173 Tennessee and northwestern Georgia (Figure 1). The CRW is an eight-digit Hydrologic
174 Unit Code (HUC08) subbasin (03150101) with a total drainage area of ~1880 km². The
175 northeastern portions of the watershed are rugged, mountainous areas largely covered
176 with forests (Ivey and Evans, 2000; Elliott and Vose, 2005). The CRW, which is one
177 headwater basin of the Alabama-Coosa-Tallapoosa (ACT) River Basin, rises high on the
178 Blue Ridge Mountains of Georgia and Tennessee and flows for 145 km before joining the
179 Coosawattee River to form the Oostanaula River (Ivey and Evans, 2000; USACE, 2013).
180 The CRW climate is characterized by warm, humid summers, and mild winters with
181 mean annual temperature of 15 to 20 °C and average annual precipitation of 1300 to 1400
182 mm (FIS, 2007; FIS, 2010; Baechler et al., 2015). The watershed encompasses four

183 counties: Bradley, Polk, Fannin, Murray, and Whitfield. It also includes the cities of
184 Dalton and Chatsworth, Georgia. There is no major reservoir located in the CRW.



185

186 Figure 1. Conasauga River Watershed study area location, model extent, electric
187 substations, and inflow locations. Background layer source: © OpenStreetMap
188 contributors 2020. Distributed under a Creative Commons BY-SA License.

189

190 2.2. Streamflow Projections

191 The ensemble streamflow projections were generated by a hierarchical modeling
192 framework, which started with regional climate downscaling followed by hydrologic
193 modeling (Gangrade et al., 2020). The climate projections were generated by dynamically
194 downscaling of 11 GCMs from the Coupled Model Intercomparison Project Phase-5
195 (CMIP5) data archive. Each GCM was used as lateral and lower boundary forcing in a
196 regional climate model RegCM4 (Giorgi et al., 2012) at a horizontal grid spacing of 18

197 km over a domain that covered continental US and parts of Canada and Mexico (Ashfaq
 198 et al., 2016) (Table 1). Each RegCM4 integration covered 40 years in the historic period
 199 (1966–2005; hereafter baseline) and another 40 years in the future period (2011–2050)
 200 under Representative Concentration Pathway 8.5 (RCP 8.5) emission scenario, with a
 201 combined 880 years of data across all RegCM4 simulations. [To capture the multi-decadal](#)
 202 [climate variability, a minimum of 30-year period has been used in many studies \(e.g.,](#)
 203 [Alfieri et al., 2015a, 2015b\).](#) [Given the additional data available from Gangrade et al.](#)
 204 [\(2020\), we have adopted a longer 40-year period that may further enlarge the sample](#)
 205 [space to better support the statistical analyses in this study.](#)
 206

207 Table 1. Summary of the 11 dynamically downscaled climate models (adopted from
 208 Ashfaq et al., 2016).

S. No.	Climate model name	Number of flood events per climate model	Time period	
1	ACCESS1-0			
2	BCC-CSM1-1			
3	CCSM4			
4	CMCC-CM			
5	FGOALS-g2		1966–2005	2011-2050
6	GFDL-ESM2M	40	(Baseline)	(Future/RCP
7	MIROC5			8.5)
8	MPI-ESM-MR			
9	MRI-CGCM3			
10	NorESM1-M			
11	IPSL-CM5A-LR			

209

210 The RegCM4 simulated daily precipitation and temperature were further statistically
211 bias-corrected to a spatial resolution of 4 km following a quantile mapping technique,
212 described in Ashfaq et al. (2010, 2013). The 4 km Parameter-elevation Regressions on
213 Independent Slopes Model (PRISM; Daly et al., 2008) data was used as the historic
214 observations to support bias-correction. In the baseline period, the simulated quantiles of
215 precipitation and temperature were corrected by mapping them onto the observed
216 quantiles. In the future period, the monthly quantile shifts were calculated based on the
217 simulated baseline and future quantiles which were subsequently added to the bias
218 corrected baseline quantiles to generate bias-corrected monthly future data. Finally, the
219 monthly bias-corrections were distributed to the daily values while preserving in each
220 time period. This approach substantially improves the biases in the modeled daily
221 precipitation and temperature while preserving the simulated climate change signal.
222 Further details of the bias-correction are provided in Ashfaq et al. (2010, 2013) while the
223 information regarding the RegCM4 configuration, evaluation and future climate
224 projections are detailed in Ashfaq et al. (2016).

225 The hydrologic simulations were then conducted using the Distributed Hydrology
226 Soil Vegetation Model (DHSVM; Wigmosta et al., 1994), which is a process-based high-
227 resolution hydrologic model that can capture heterogeneous watershed processes and
228 meteorology at a fine resolution. DHSVM uses spatially distributed parameters, including
229 topography, soil types, soil depths, and vegetation types. The input meteorological data
230 includes precipitation, incoming shortwave and longwave radiation, relative humidity, air
231 temperature and wind speed (Wigmosta et al., 1994; Storck et al., 1998; Wigmosta et al.,
232 2002). The DHSVM performance and applicability has been reported in various earlier

233 climate and flood related studies (Elsner et al., 2010; Hou et al., 2019; Gangrade et al.,
234 2018, 2019, 2020). A calibrated DHSVM implementation from Gangrade et al. (2018) at
235 90 m grid spacing was used to produce 3-hourly streamflow projections using the
236 RegCM4 meteorological forcings described in the previous section (Table 1). In addition,
237 a control simulation driven by 1981–2012 Daymet meteorologic forcings (Thornton et
238 al., 1997) was conducted for model evaluation and validation. The hydrologic simulations
239 used in this study are a part of a larger hydroclimate assessment effort for the ACT River
240 Basin, as detailed in Gangrade et al. (2020). Since there is no major reservoir in the
241 CRW, the additional reservoir operation module (Zhao et al., 2016) was not needed in
242 this study.

243 Note that while the ensemble streamflow projections based on dynamical
244 downscaling and high-resolution hydrologic modeling from Gangrade et al. (2020) are
245 suitable to explore extreme hydrologic events in this study, they do not represent the full
246 range of possible future scenarios. Additional factors such as other GCMs, RCP
247 scenarios, downscaling approaches, and hydrologic models and parameterization may
248 also affect future streamflow projections. In other words, although these ensemble
249 streamflow projections can tell us how likely the future streamflow magnitude may
250 change from the baseline level, they are not the absolute prediction into the future. In
251 practice, these modeling choices will likely be study-specific based on the agreement
252 among key stakeholders. It is also noted that the new Coupled Model Intercomparison
253 Project Phase-6 (CMIP6) data have also become available to update the ensemble
254 streamflow projections, but is not pursued in this study.

255 **2.3. Inundation Modeling**

256 The ensemble inundation modeling was performed using TRITON, which is a
257 computationally enhanced version of Flood2D-GPU (Kalyanapu et al., 2011). TRITON
258 allows parallel computing using multiple graphics processing units (GPUs) through a
259 hybrid Message Passing Interface (MPI) and Compute Unified Device Architecture
260 (CUDA) (Morales-Hernández et al., ~~2020b~~2021). TRITON solves the nonlinear
261 hyperbolic shallow water equations using an explicit upwind finite-volume scheme,
262 based on Roe's linearization. The shallow water equations are a simplified version of the
263 Navier-Stokes equations in which the horizontal momentum and continuity equations are
264 integrated in the vertical direction (see Morales-Hernández et al., (~~2020b~~2021), for
265 further model details). An evaluation of TRITON performance for the CRW is presented
266 and discussed in Section 3.3.

267 TRITON's input data includes digital elevation model (DEM), surface roughness,
268 initial depths, flow hydrographs, and inflow source locations (Kalyanapu et al., 2011;
269 Marshall et al., 2018; Morales-Hernández et al., 2020a; Morales-Hernández et al.,
270 ~~2020b~~2021). In this study, the hydraulic and geometric parameters from the flood model
271 evaluation section (Section 3.3) were used in the flood simulation. The topography was
272 represented using the one-third arc-second (~10 m) spatial resolution DEM (Archuleta et
273 al., 2017) from the US Geological Survey (USGS). To improve the quality of the base
274 DEM, as discussed in the flood model evaluation section, the main channel elevation was
275 reduced by 0.15 m. Elevated roads and bridges that obstruct the flow of water were also
276 removed. For surface roughness, we used a single channel Manning's n value of 0.05 and
277 a single floodplain Manning's n value of 0.35. The selection of channel and floodplain
278 Manning's n value was based on the Whitfield County Flood Insurance Study (FIS,

279 2007), which reported a range of Manning's n values estimated from field observations
280 and engineering judgment for about 15 streams inside the CRW (section 3.2).
281 Furthermore, a water depth value of 0.35 m was defined for the main river channel as an
282 initial boundary condition. The zero velocity gradients were used as the downstream
283 boundary condition. Further discussion of model parameter sensitivity and model
284 evaluation are provided in sections 3.2 and 3.3.

285 The simulated DHSVM streamflow was used to prepare inflow hydrographs for
286 ensemble inundation modeling. To provide a large sample size for frequency analysis, we
287 selected all annual maximum peak streamflow events (the maximum corresponded to the
288 outlet of CRW [Figure 1]) from the 1981–2012 control simulation (32 years), the 1966–
289 2005 baseline simulation (440 years; 40 years \times 11 models), and the 2011–2050 future
290 simulation (440 years; 40 years \times 11 models), with a total of 912 events. For each annual
291 maximum event, the 3-hour timestep, 10-day hydrographs (which capture the peak CRW
292 outlet discharge) across all DHSVM river segments were summarized. Following a
293 procedure similar to Gangrade et al. (2019), these streamflow hydrographs were
294 converted to TRITON inputs at 300 inflow locations selected along the NHD+ river
295 network in the CRW (Figure 1). The TRITON model extent, shown in Figure 1, has an
296 approximate area of 3945 km² and includes ~44 million model grid cells (7976 rows \times
297 5474 columns in a uniform structured mesh). The ensemble flood simulations resulted in
298 gridded flood depth and velocity output at 30-minute intervals. The simulations generated
299 an approximately 400 Terabyte data and utilized ~2000 node hours on the Summit
300 supercomputer, managed by the Oak Ridge Leadership Computing Facility at Oak Ridge
301 National Laboratory.

302 **2.4. Flood Inundation Frequency Analysis**

303 Given the nature of GCM experiments, each set of climate projections can be
304 considered as a physics-based realization of historic and future climate under specified
305 emission scenarios. Therefore, an ensemble of multimodel simulations can effectively
306 increase the data lengths and sample sizes that are keys to support frequency analysis,
307 especially for low-AEP events. In this study, we conducted flood frequency analyses
308 separately for the 1966–2005 baseline and 2011–2050 future periods so that the
309 difference between the two periods represent the changes in flood risk due to climate
310 change.

311 To prepare the flood frequency analysis, we first calculated the maximum flood depth
312 at every grid in each simulation. A minimum threshold of 10 cm flood depth was used to
313 judge whether a cell was wet or dry (Gangrade et al., 2019). Further, for a given grid cell,
314 if the total number of non-zero flood depth values (i.e., of the 440 depth values) was less
315 than 30, the grid cell was also considered dry. This threshold was selected based on the
316 minimum sample size requirement for flood depth frequency analysis suggested by Li et
317 al. (2018). Next, we calculated the maximum flooded area (hereafter used alternatively
318 with “floodplain area”) for each simulation. A log-Pearson Type III (LP3) distribution
319 was then used for frequency analysis following the guidelines outlined in Bulletins 17B
320 (USGS, 1982; Burkey, 2009) and 17C (England Jr. et al., 2019). Two types of LP3 fitting
321 were performed. The first type of fitting is event-based that fitted LP3 on the maximum
322 inundation area across all ensemble members. The second type of fitting is grid-based
323 (more computationally intensive) that fitted LP3 on the maximum flood depth at each
324 grid cell across all ensemble members. For both types of fittings, the frequency estimates

325 at 4%, 2%, 1%, and 0.5% AEP (corresponding to 25-, 50-, 100-, and 200-year return
326 levels) were derived for further analysis.

327 It is also noted that in addition to the annual maximum event approach used in this
328 study, one may also use the peak-over-threshold (POT) approach which can select
329 multiple streamflow events in a very wet year. While such an approach can lead to higher
330 extreme streamflow and inundation estimates, the timing of POT samples is fully
331 governed by the occurrences of wet years. In other words, if the trend of extreme
332 streamflow is significant in the future period, the POT samples will likely occur more in
333 the far future period. We hence select the annual maximum event approach that can
334 sample maximum streamflow events more evenly in time, which can better capture the
335 evolution of extreme events with time under the influence of climate change.

336 **2.5. Vulnerability of Electricity Infrastructure**

337 The vulnerability of electricity infrastructures to climate change-induced flooding
338 was evaluated using the ensemble flood inundation results. The 44 electric substations
339 (Figure 1) collected from the publicly available Homeland Infrastructure Foundation-
340 Level Data (HIFLD, 2019) were considered to be the electrical components susceptible to
341 flooding. To evaluate the vulnerability of these substations, we overlapped the maximum
342 flood extent from each ensemble member with all substations to identify the substations
343 that might be inundated under the baseline and future climate conditions. Further, as an
344 additional flood hazard indicator, the duration of inundation was estimated at each of the
345 affected substations using the ensemble flood simulation results.

346 The vulnerability analysis was performed for two different flood mitigation scenarios.
347 In the first scenario, we assumed that no flood protection measures were provided at all

348 substations. Hence, the substations that intersected with the flood footprint were
349 considered to be failed. In the second scenario, it was assumed that flood protection
350 measures were adopted for all substations following the FEMA P-1019 recommendation
351 (FEMA, 2014). According to FEMA P-1019 (FEMA, 2014), for emergency power
352 systems within critical facilities, the highest elevation among (1) the base flood elevation
353 (BFE: 1% FEMA AEP flood elevation) plus 3 feet (~0.91 m), (2) the locally adopted
354 design flood elevation, and (3) the 500-year flood elevation can be used to design flood
355 protection measures. Since the three recommended elevations were not available at all
356 substation locations, we focused only on the BFE plus ~0.91 m option. In addition, since
357 in the CRW the majority of existing flood insurance maps were classified as Zone A—
358 meaning that the special flood hazard areas were determined by approximate methods
359 without BFE values (FEMA, 2002)—we used the maximum flood depth values across all
360 control simulation years as the BFE values in this second mitigation scenario.

361 During the vulnerability analysis, we also assumed that (1) the one-third arc-second
362 spatial resolution DEM might reasonably represent the elevation of substations, (2)
363 existing substations would remain functional and would not be relocated, and (3) no
364 additional hardening measures (i.e., protections such as levees, berms, anchors, and
365 housings) will be adopted in the future period. Also, the cascading failure of a substation
366 due to grid interconnection was not considered in this study.

367

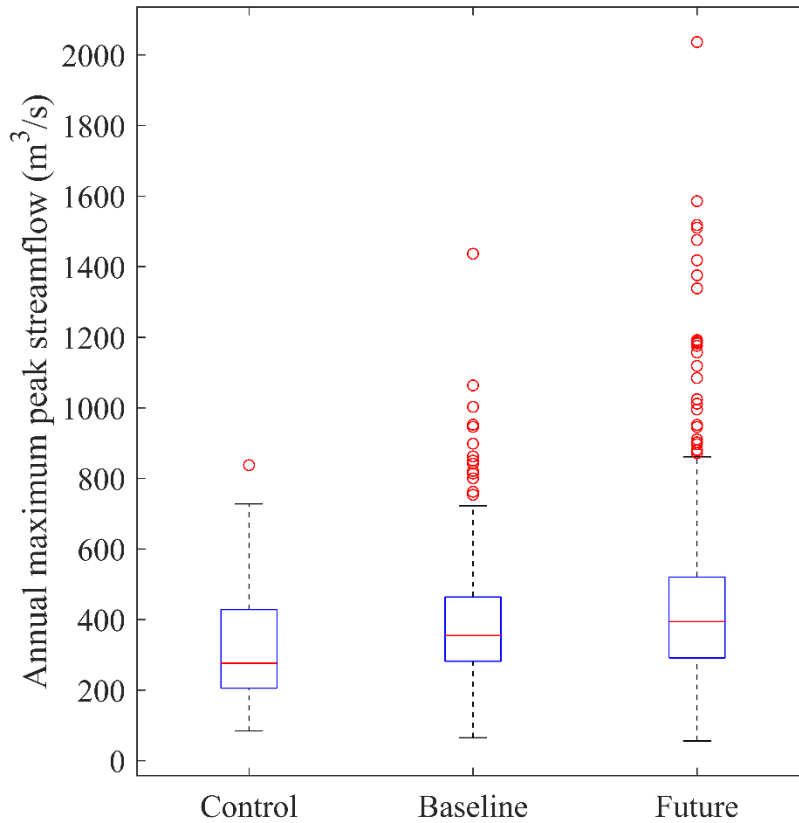
368 **3. Results and Discussion**

369 **3.1. Streamflow Projections**

370 This section presents a comparison of the annual maximum peak streamflow (at the
371 outlet of CRW) used in the control, baseline, and future simulations. The sample size
372 included 32 events from the control (1981–2012) simulation, 440 events from the
373 baseline (1966–2005) simulations, and another 440 events from the future (2011–2050)
374 simulations. These samples are illustrated in box and whisker plots in Figure 2, where
375 central mark indicate the median, while bottom and top edges indicate the 25th and 75th
376 percentiles respectively. The whiskers extend to the furthest data points not considered
377 outliers, which correspond to approximately ± 2.7 standard deviations and 99.3%
378 coverage if the data are normally distributed. As is evident from Figure 2, the
379 distributions of annual maximum peak streamflow values in the control and baseline
380 simulations are comparable. The upper and lower whiskers in the control simulation are
381 727.6 m³/s and 84.2 m³/s, which compare well to the 722.5 m³/s and 65.2 m³/s values in
382 the baseline simulation. In addition, we also conducted a two-tailed two-sample t-test (α
383 = 0.05) to compare if the means of control and baseline annual maximum streamflow are
384 statistically different. The results yielded a p-value of 0.09 which suggested that there is
385 no significant difference between the means of both control and baseline simulations. A
386 larger number of outliers are present in the baseline simulation, which is due to the larger
387 sample size (440 versus 32).

388 Under the future projection, an increase in the maximum peak streamflow is shown,
389 where the upper whisker in the future projection is ~21% higher than the baseline.
390 Moreover, the maximum of distribution in the future climate (2036.7 m³/s) is also much
391 higher than that in the baseline climate (1436.7 m³/s), suggesting a higher future flood

392 risk in the CRW. The increasing trend of streamflow extremes in the CRW is consistent
393 with the overall findings in the ACT River Basin (Gangrade et al., 2020).



394
395 Figure 2. A comparison of annual maximum peak streamflow at the outlet of Conasauga
396 River Watershed. The sample size includes 32 events from the control (1981–2012), 440
397 from the baseline (1966–2005), and another 440 from the future (2011–2050) periods.

398 3.2. Sensitivity Analysis for Flood Model

399 For a better understanding and selection of suitable TRITON parameters, a series of
400 sensitivity analyses were conducted using different combinations of Manning’s
401 roughness, initial water depths, and river bathymetry correction factors (Table 2).

402

403

404

405 Table 2. Summary of hydraulic and geometric parameters used in the sensitivity analysis.

Sensitivity parameter	Scenario	Initial water depth values (m)	Surface roughness (Manning's n values)	Bathymetry correction factor (m)
Initial water depth	1	0.00	$n_{ch} = 0.050 / n_{fldpl} = 0.350$	-0.15
	2	0.15		
	3	0.35		
	4	0.45		
	5	0.55		
	6	0.65		
Surface roughness	1	0.35	N_1: $n_{ch} = 0.035 / n_{fldpl} = 0.06$	-0.15
	2		N_2: $n_{ch} = 0.040 / n_{fldpl} = 0.25$	
	3		N_3: $n_{ch} = 0.045 / n_{fldpl} = 0.30$	
	4		N_4: $n_{ch} = 0.050 / n_{fldpl} = 0.35$	
	5		N_5: $n_{ch} = 0.055 / n_{fldpl} = 0.45$	
	6		N_6: $n_{ch} = 0.060 / n_{fldpl} = 0.50$	
Bathymetry correction factor	1	0.35	$n_{ch} = 0.050 / n_{fldpl} = 0.350$	0.00
	2			-0.15
	3			-0.45
	4			-0.75
	5			-1.00
	6			-1.25

406 Note: n_{ch} represents the Manning's n value in the main channel and n_{fldpl} represents the
407 Manning's n value in the floodplain areas.

408

409 In calibrating a hydraulic model, it is a common practice to adjust the estimated
410 Manning's n value, as it is the most uncertain and variable input hydraulic parameter
411 (Brunner et al., 2016). In this study, we tested six different scenarios (Table 2) based on
412 the Whitfield County Flood Insurance Study (FIS, 2007), which reported a range of
413 Manning's n values estimated from field observations and engineering judgment for
414 about 15 streams inside the CRW. It is noted that the depth variation of Manning's
415 roughness is not considered in the current study. Readers are referred to studies such as

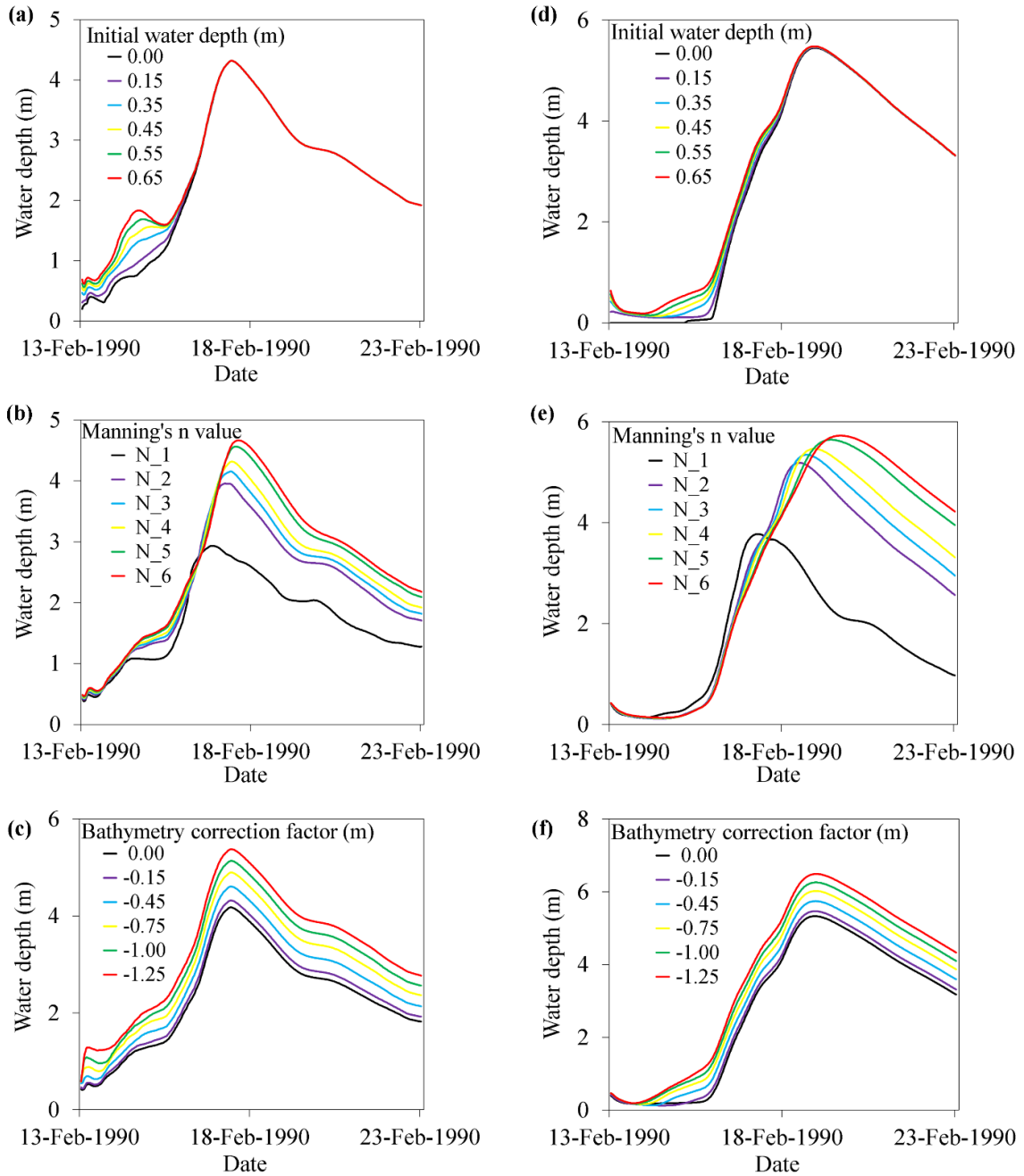
416 [Saksena et al. \(2020\) for additional information on the dynamic Manning's roughness for](#)
417 [potential hydrology and hydraulics applications.](#)

418 To establish an initial condition for TRITON, a sensitivity analysis was performed on
419 selected initial water depth values (ranging from 0 m to 0.65 m, Table 2) to understand
420 their relative effects. To select ranges for the initial water depth, we summarized the
421 observed water depth values that corresponds to low flow values at five USGS gauge
422 stations inside the CRW. The distribution of observed water depth values from the five
423 gauges showed average values ranging from 0.25 to 0.65m. Existing DEM products, even
424 those with high spatial resolution (i.e., 10 m or finer), do not represent the elevation of
425 river bathymetry accurately (Bhuyian et al., 2014). For the CRW, Bhuyian et al. (2019)
426 found that the one-third arc-second spatial resolution base DEM over-predicted the
427 inundation extent because of the bathymetric error, which reduced the channel
428 conveyance. In this study, we tested various bathymetry correction factors (ranging from
429 -1.25 m to 0 m, Table 2) by reducing the DEM elevation along the main channel to
430 understand the sensitivity of TRITON.

431 The sensitivity analysis was performed using the February 13–22, 1990 flood event
432 that has the maximum discharge among all 32 control simulation events. To evaluate
433 relative sensitivity of TRITON, we extracted simulated flood depths at two arbitrary
434 selected locations (Figure 1) and estimated the relative inundation area differences. The
435 impacts of initial water depths were significant only at the beginning where low flow
436 values dominated the hydrographs (Figure 3a, 3d). Larger initial water depth values
437 generated higher flood inundation depths for both sample locations. Although the
438 differences in flood inundation extents relative to the dry bed show an increasing trend,

439 the relative differences are less than 1.4% (Figure 4a). Increase in the channel and
440 floodplain Manning's n values resulted in higher flood depths for both sample locations
441 (Figure 3b and 3e). The relative flood inundation area differences increase from about
442 23% to 31% (Figure 4b) when the channel and floodplain Manning's n values are
443 increased from 0.035 to 0.06 and from 0.06 to 0.50, respectively. Reduction in the
444 elevation of river bathymetry (to improve the quality of the base DEM) results in a direct
445 increase in maximum flood depth due to change in the river conveyance (Figure 3c and
446 3f). It also results in a decrease in the maximum flood extent (Figure 4c), as more water
447 is allowed to transport through the main channel instead of the floodplain. A similar
448 phenomenon was observed in other studies including Dey et al., (2019). Overall, the
449 results showed that TRITON was more sensitive to the Manning's n values than the
450 initial water depths and bathymetric correction factors.

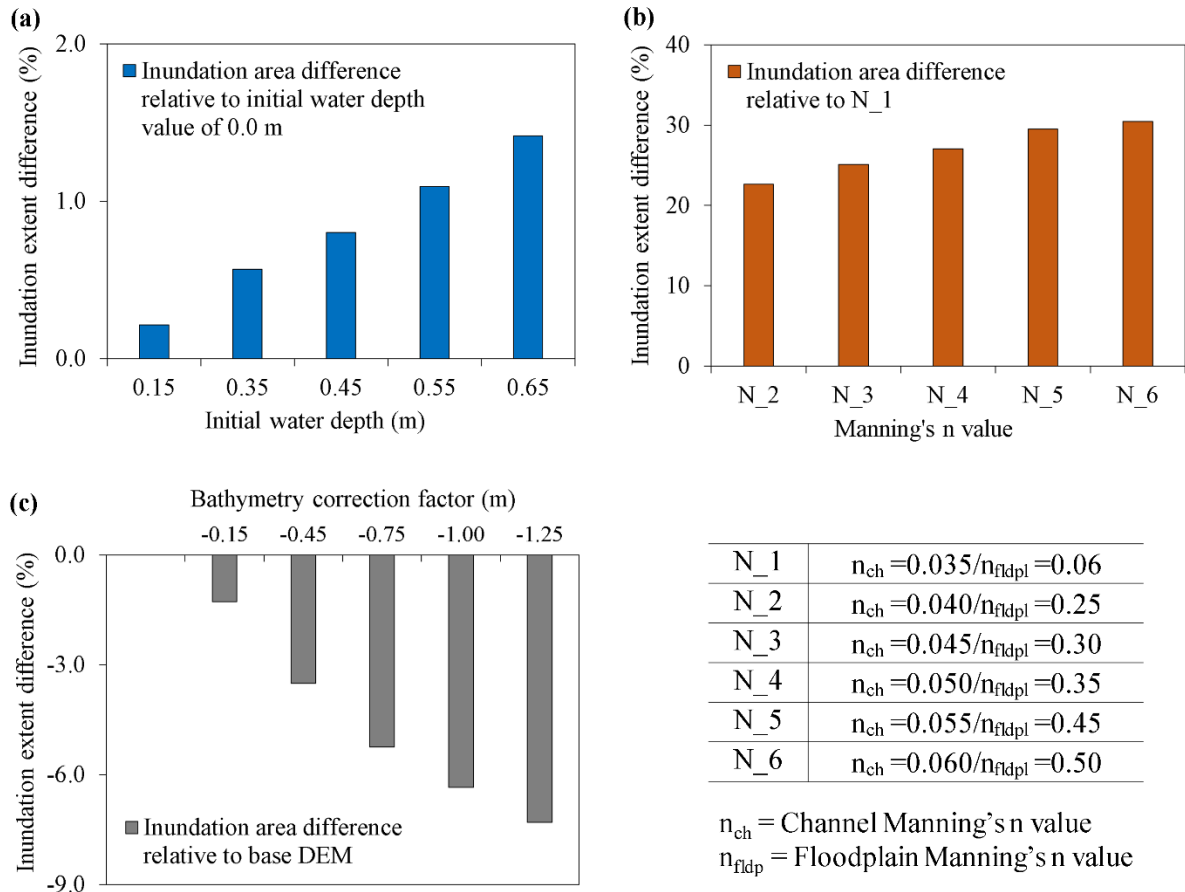
451



452

453 Figure 3. Simulated flood inundation depths extracted at location 1 (a, b, c) and at
 454 location 2 (d, e, f). Note: Location 1 and 2 are shown in Figure 1. A description of the
 455 Manning's n values (N_1 to N_6) can be found in Table 2.

456



457

458 Figure 4. Change in simulated maximum flood inundation extents for (a) initial water
 459 depth, (b) Manning's n value, and (c) bathymetry correction factor.

460

461 3.3. Flood Model Evaluation

462 Because of a lack of observed streamflow data in the CRW, the performance of
 463 TRITON was evaluated by comparing the simulated 1% AEP flood map with the
 464 published 1% AEP flood map from FEMA (FEMA, 2019). The purpose of this
 465 assessment is to understand whether TRITON can provide comparable results to the
 466 widely accepted FEMA flood estimates. While the FEMA AEP flood maps do not
 467 necessarily represent complete ground truth, such a comparison is the best option given

468 the data challenge. Similar approach has been utilized by several previous studies in the
469 evaluation of large-scale flood inundation evaluation (Alfieri et al., 2014; Wing et al.,
470 2017; Zheng et al., 2018; Gangrade et al., 2019).

471 To derive the 1% AEP flood map using TRITON, the ensemble-based approach used
472 by Gangrade et al. (2019) was followed. The assessment started by preparing the
473 streamflow hydrographs used to construct the 1% AEP flood map. The 1981–2012
474 annual maximum peak events and their corresponding 10-day streamflow hydrographs
475 were extracted from the control simulation. These streamflow hydrographs were then
476 proportionally rescaled to match the 1% AEP peak discharge estimated at the watershed
477 outlet (Figure 1), following the frequency analysis procedures outlined in Bulletin 17C
478 (England Jr. et al., 2019). The streamflow hydrographs from control simulations were
479 used for the peak discharge frequency analysis.

480 The results reported in the sensitivity analysis were also used to help identify suitable
481 TRITON parameters. In addition to streamflow hydrographs, TRITON requires DEM,
482 initial water depth, and Manning's n value. To minimize the effect of bathymetric error in
483 the base DEM (Bhuyian et al., 2014; Bhuyian et al., 2019), we reduced the elevation
484 along the main channel by 0.15 m (i.e., a bathymetry correction factor). Although this
485 simple approach is unlikely to adjust the channel bathymetry to its true values, it can
486 improve the channel conveyance volume that is lost in the base DEM. To further improve
487 the quality of the base DEM, we removed elevated roads and bridges that could obstruct
488 the flow of water in some of the streams and rivers. An initial water depth of 0.35 m was
489 also selected in this study. For the surface roughness, a couple of flood simulations were
490 performed by adjusting the Manning's n values for the main channel and floodplain to

491 achieve satisfactory agreement between the simulated and the reference FEMA flood
492 map. We eventually selected a single channel Manning's n value of 0.05 and a single
493 floodplain Manning's n value of 0.35.

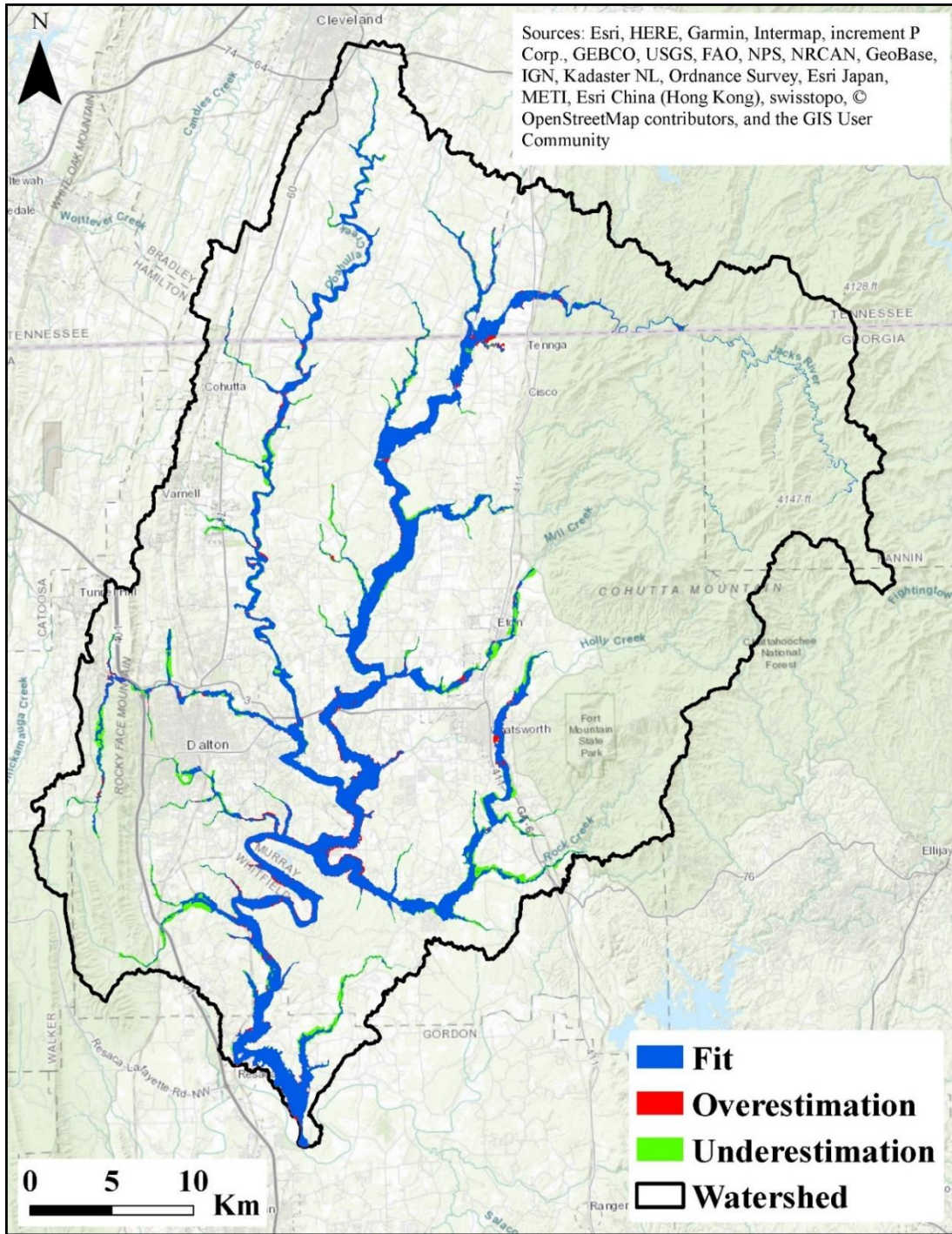
494 Three evaluation metrics, including fit, omission, and commission (Kalyanapu et al.,
495 2011) were used to quantify the differences between the modeled and reference flood
496 map. The measure of fit determines the degree of relationship, while the omission and
497 commission statistically compare the simulated and reference FEMA flood maps
498 (Kalyanapu et al., 2011). The comparison between the simulated maximum inundation
499 and the corresponding 1% AEP FEMA flood map showed 80.65% fit, 5.52%
500 commission, and 15.36% omission (Figure 5), demonstrating that the TRITON could
501 reasonably estimate flood inundation extent, and depths, ~~and velocities~~ in the CRW. The
502 computational efficiency of TRITON can further support ensemble inundation modeling
503 to provide additional variability information that cannot be provided by the conventional
504 deterministic flood map.

505 Although we have obtained satisfactory model performance for the purpose of our
506 study, the flood model implementation has some limitations that may be enhanced in
507 future studies. They include:

- 508 • Spatially varying Manning's n values may be derived based on high-resolution
509 land use land cover (LULC) conditions to better represent the spatial
510 heterogeneity in the modeling domain.
- 511 • Apart from changes in future runoff and streamflow, projections of future LULC
512 and its corresponding surface roughness can be considered to understand the
513 broader impacts due to environment change.

514
515
516
517
518
519
520
521
522
523
524
525

- In this study, we corrected DEM bias along the river channel cells by simplified bathymetry correction factors. More sophisticated bathymetric configuration (i.e., channel shape and sinuosity) can be considered to better represent channel conveyance.
- The current TRITON model does not provide capability to route local runoff and external inflows through stormwater drainage systems. Coupling with additional stormwater drainage models can be a potential future direction.
- Hydraulic and civil structures such as bridges, culverts, and weirs have not been included since TRITON does not provide for the modeling of such components. This can affect the accuracy of the flood depths, velocities, and flood extents around these structures.



526

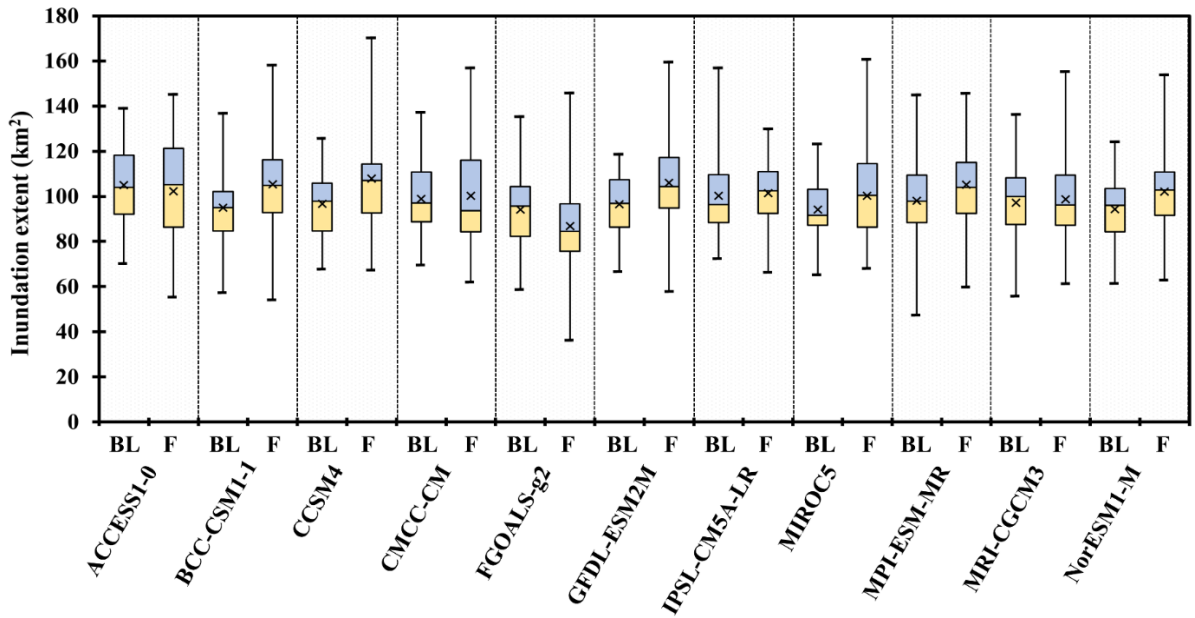
527 Figure 5. Comparison of simulated maximum flood extent with the corresponding FEMA
 528 1% AEP flood map for the Conasauga River Watershed. Background layer source: ©
 529 OpenStreetMap contributors 2020. Distributed under a Creative Commons BY-SA
 530 License.

531

532 **3.4. Change in Flood Regime**

533 In this section, the projected changes in flood regime were calculated using the
534 flooded area from the baseline and future simulations for each ensemble member. Figure
535 6 illustrates the box and whisker plots for each of the 11 dynamically downscaled GCMs.
536 Given the small sample size in each distribution (40 compared to 440 in Figure 2), the
537 whiskers extend the largest/smallest data points with no outlier detection. For 9 out of the
538 11 downscaled climate models, the mean of 40 flood inundation showed an increase in
539 the floodplain area in the future period. In terms of the 75th percentile and maximum, 10
540 out of 11 models showed increase in the floodplain area. The distribution of maximum
541 future inundation of 4 models are found to be statistically different than their baseline
542 distributions at a 5% significance level. Note that the spread in the future period is
543 generally larger than the spread in the baseline period, suggesting an increase in the
544 hydrologic variability in the future period. Also, while the results from different models
545 were generally consistent, some inter-model differences were noted, which highlight the
546 need of a multi-model framework to capture the uncertainty in the future climate
547 projections. The multi-model approach provides a range of possible flood inundation
548 extents, which is critical for floodplain management decision making. The potential
549 increase in the floodplain area also demonstrates the importance of incorporating climate
550 change projections in the floodplain management regulations.

551



552

553 Figure 6. A summary of simulated maximum flood inundation extents obtained from the
 554 baseline and future scenarios. The mean flooded area values are shown by × symbols.

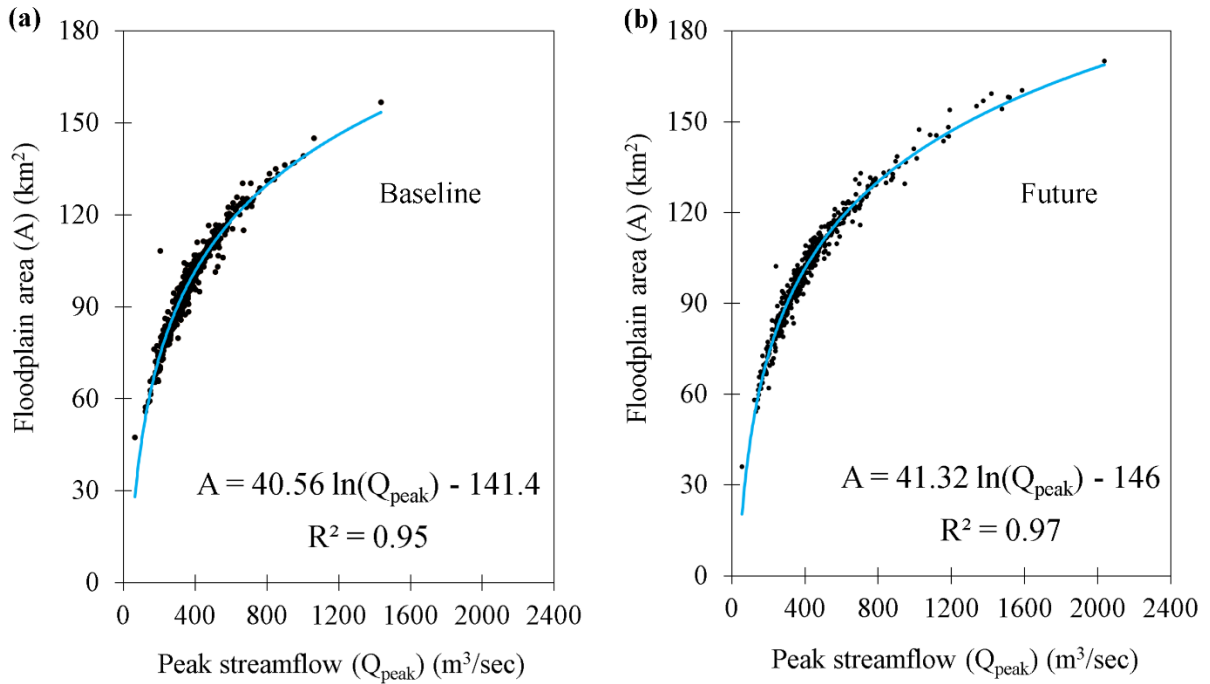
555 Note: The suffix “_BL” represents baseline scenarios and the suffix “_F” represents
 556 future scenarios.

557 **3.5. Flood Inundation Frequency Curve and Map**

558 Figure 7 shows the relationship between the 440 flooded area values (across 11
 559 downscaled GCMs) and their corresponding peak streamflow at the watershed outlet, for
 560 both the baseline and future periods. Overall, both results (Figure 7a and 7b) exhibit
 561 strong nonlinear relationships with high R² values. The results suggest that peak
 562 streamflow is a significant variable controlling the total flooded area, but the variability
 563 of flooded area could not be explained by peak streamflow alone. For instance, in the
 564 baseline period, the peak streamflow values of 423.63 m³/sec and 424.25 m³/sec
 565 correspond to 106.85 km² and 94.89 km² floodplain areas, respectively (Figure 7a).

566 Similarly, in the future period, the peak streamflow values of 433.27 m³/sec and 434.21
567 m³/sec correspond to 110.76 km² and 99.26 km² floodplain areas (Figure 7b).

568



569

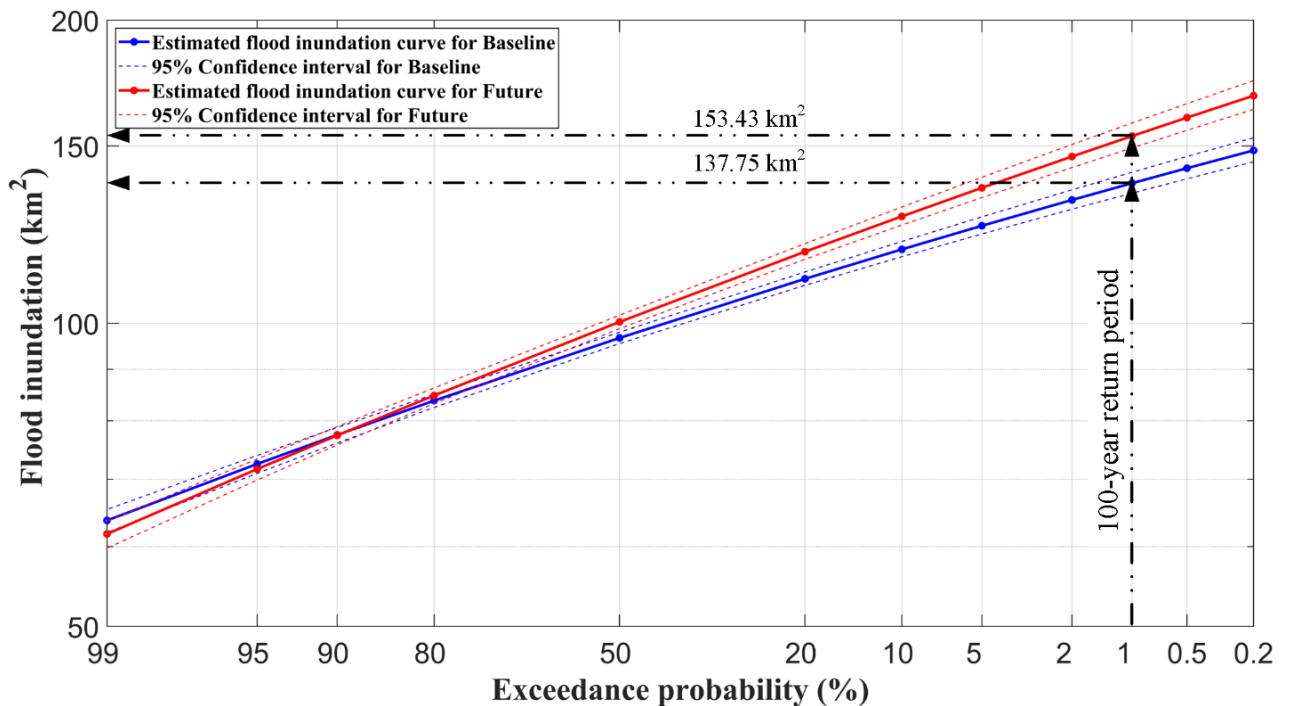
570 Figure 7. Relationship between floodplain areas and peak streamflow values at the
571 watershed outlet for (a) baseline and (b) future scenarios. The blue lines indicate the
572 logarithmic best-fit.

573

574 Figure 8 shows the event-based flood inundation frequency curves and their
575 corresponding 95% confidence intervals in both the baseline and future periods, for
576 which each frequency curve was derived using an ensemble of 440 years of data. The use
577 of long-term data helped reduce the uncertainty and add more confidence in the
578 evaluation of the lower AEP estimates. This type of assessment cannot be achieved using
579 only historic streamflow observations, for which the limited records present a major

580 challenge for lower AEP estimates. For most of the exceedance probabilities, the flooded
 581 areas projected an increase in the inundation areas in the future period when compared to
 582 the baseline period. The 1% AEP flood shows an ~16 km² increase in the inundation area
 583 (137.75 km² in the baseline period versus 153.43 km² in the future period) (Figure 8).
 584 Similar results can be observed in inundation frequency curves developed for other AEPs
 585 (not shown).

586



587

588 Figure 8. A summary of flood inundation frequency curves for the baseline and future
 589 periods.

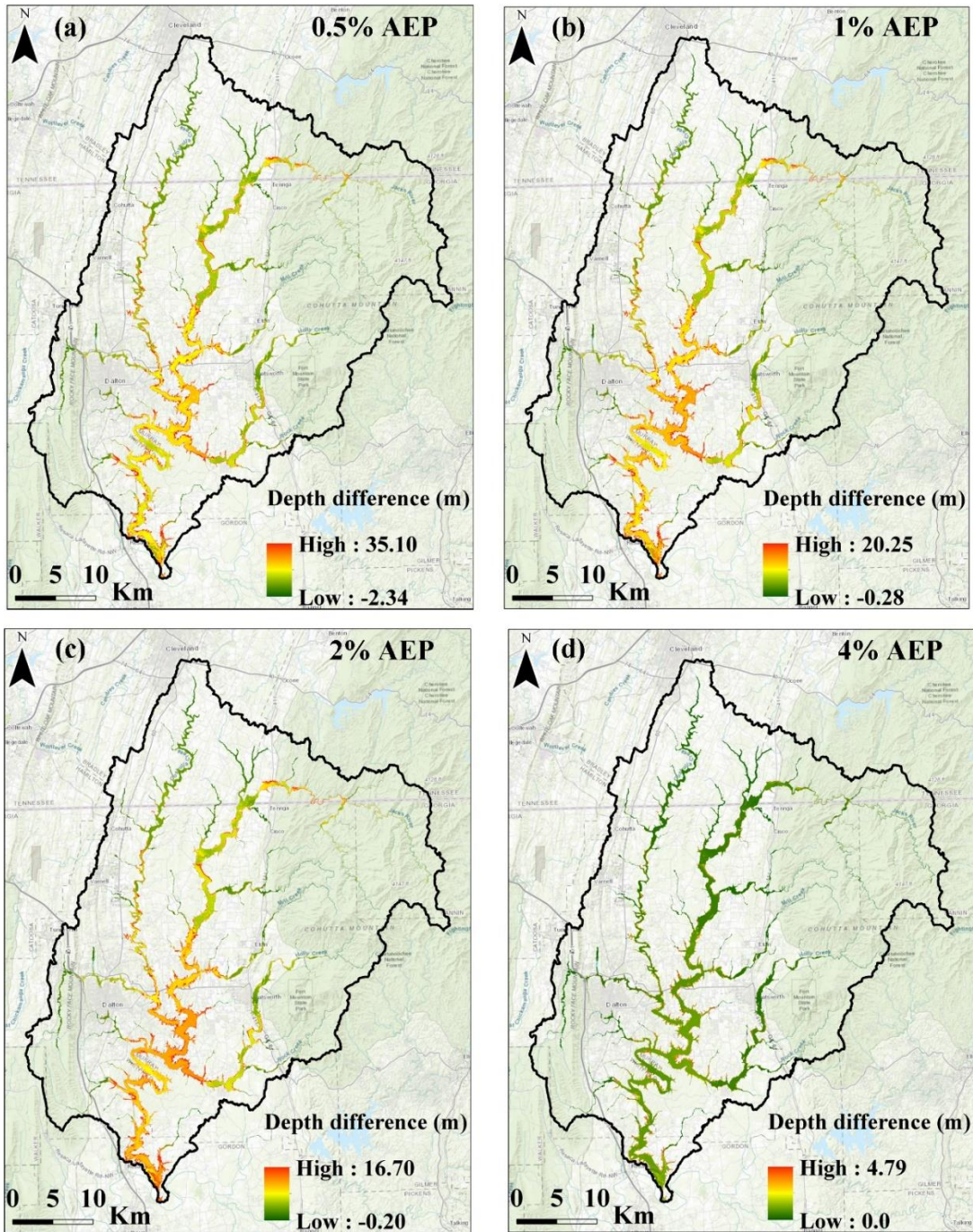
590

591 The grid-based flood depth frequency results at 0.5%, 1%, 2%, and 4% AEP levels
 592 are illustrated in Figure 9. In each panel, the projected change (i.e., future minus baseline)
 593 at each grid is shown. The corresponding histogram across the entire study area is

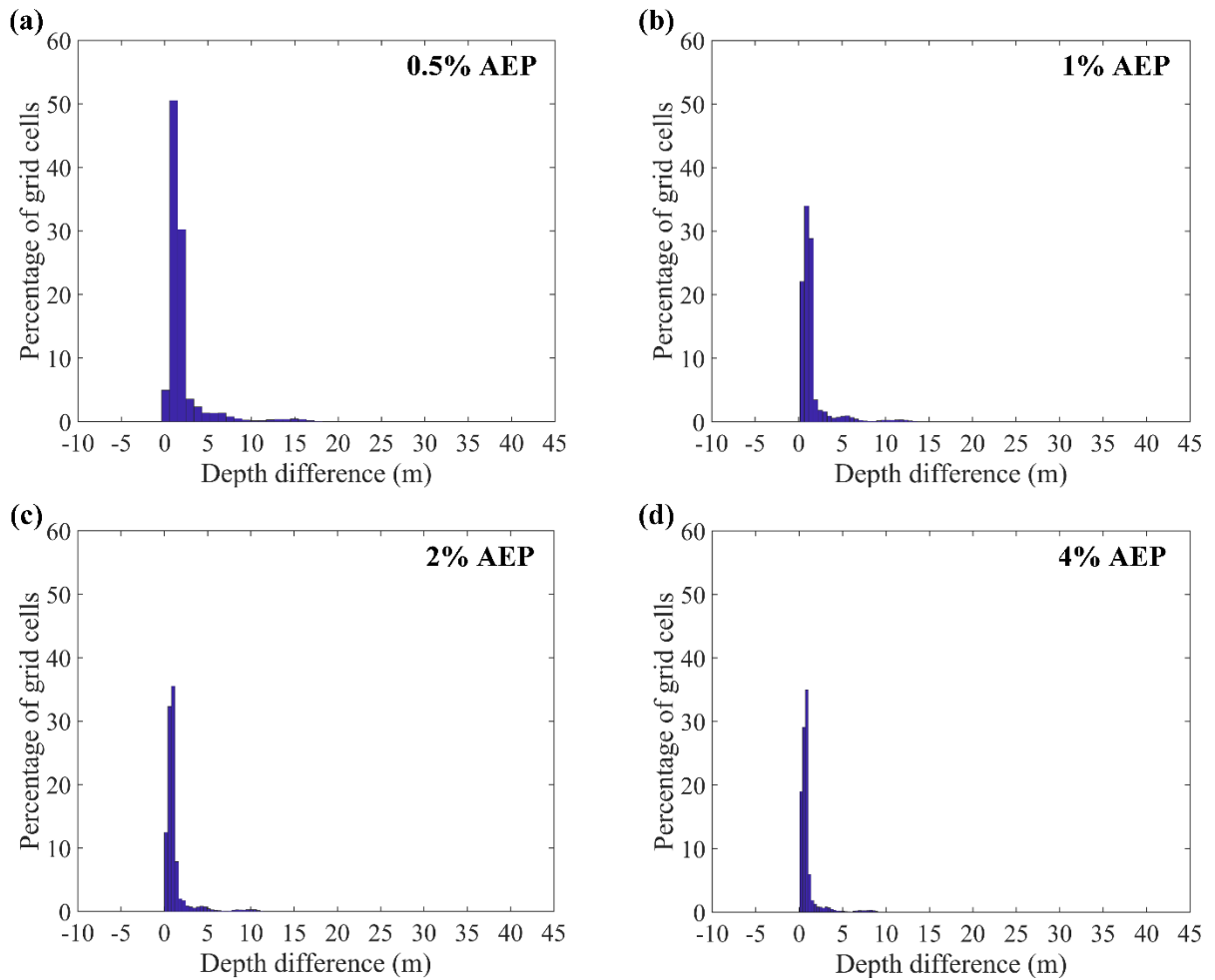
594 presented in Figure 10. As mentioned in section 2.4, the LP3 distribution was used for
595 frequency analysis. In order to understand the suitability of LP3, we also conducted a
596 comparative analysis to test an alternative log-normal (LN) distribution. By using the
597 Anderson-Darling (Anderson and Darling, 1954) goodness-of-fit test ($\alpha = 0.05$) along
598 with the Akaike Information Criteria (Akaike, 1974), we found no substantial difference
599 between these two distributions (not showed), for the purpose of our application. It is
600 noted, however, that our goal in this study is not to identify the most suitable choice of
601 flood depth distribution-of flood depth. Therefore, there can be other more suitable
602 distributions may exist but this is outside beyond the scope of this study.

603 Based on these comparisons in Figure 10, it is estimated that the flood depth values at
604 ~80% of grid cells would increase by 0.2 to 1.5 m due to projected changes in climate
605 (Figure 10). For 0.5% and 1% AEP flood depth frequency maps (Figure 9a and 9b), the
606 changes in flood depth were more pronounced in the lower part of the CRW, near the
607 City of Dalton (where there are large population settlements), thereby increasing the
608 likelihood of population exposure to flood risk in the future period. Furthermore, for the
609 1% flood depth frequency map (Figure 9b), the projected increase in flood depths and
610 spatial extent has the potential to extend the flood damage far beyond the FEMA's
611 current base floodplain area. Therefore, these results highlight the need for climate
612 change consideration in the floodplain mapping. The approach presented in this study can
613 provide an alternative floodplain delineation technique, as it can be applied to develop
614 flood depth frequency maps that are reflective of the future climate.

615



616
 617 Figure 9. Projected change (future minus baseline period) in flood depth frequency maps
 618 for (a) 0.5%, (b) 1%, (c) 2%, and (d) 4% AEPs. ArcGIS background layer sources: ESRI,
 619 HERE, Garmin, Intermap, GEBCO, USGS, Food and Agriculture Organization, National
 620 Park Service, Natural Resources Canada, GeoBase, IGN, Kadaster NL, Ordnance Survey,
 621 METI, Esri Japan, Esri China, the GIS User Community, and © OpenStreetMap
 622 contributors 2020. Distributed under a Creative Commons BY-SA License.



623

624 Figure 10. Histograms for the future changes (2011–2050) in the flood depth relative to
 625 the baseline period (1966–2005) for (a) 0.5%, (b) 1%, (c) 2%, and (d) 4% AEP flood
 626 depth frequency maps.

627

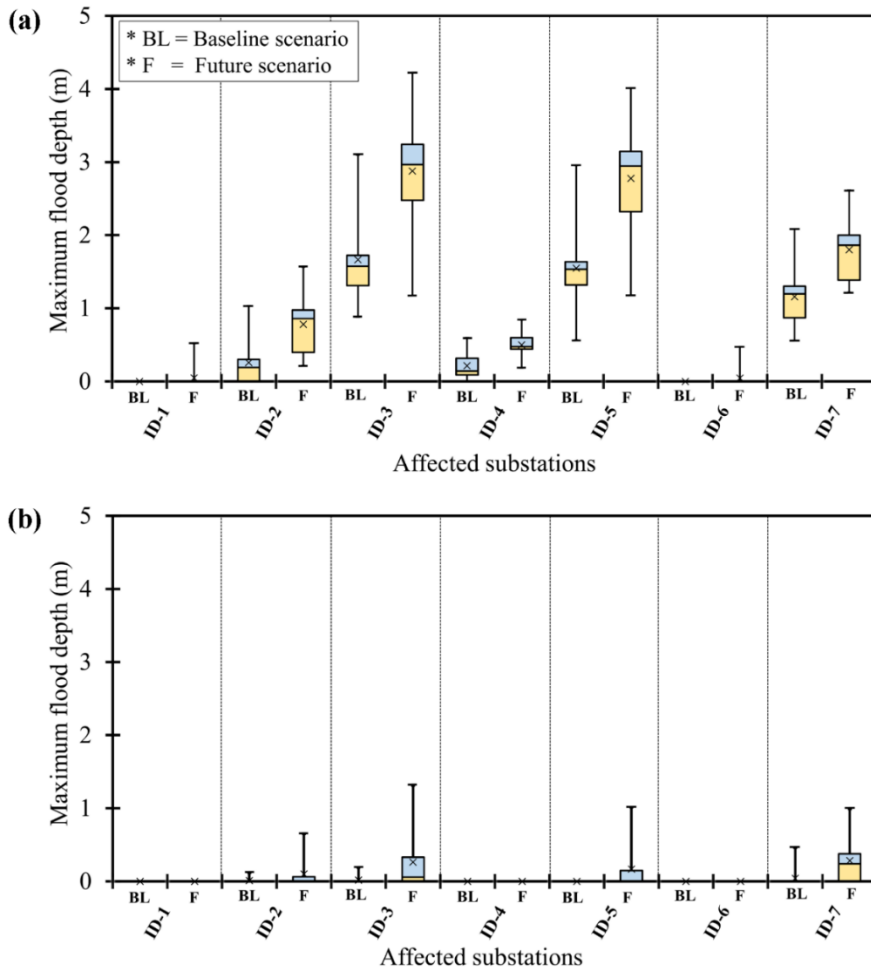
628 3.6. Vulnerability of Electricity Infrastructure

629 Figure 11a shows the box and whisker plot for the distributions of maximum flood
 630 depth values extracted at the substation location across all the baseline and future
 631 simulations, assuming that no flood protection measures were adopted (mitigation
 632 scenario 1). Of the 44 substations, 5 substations could have been affected during the

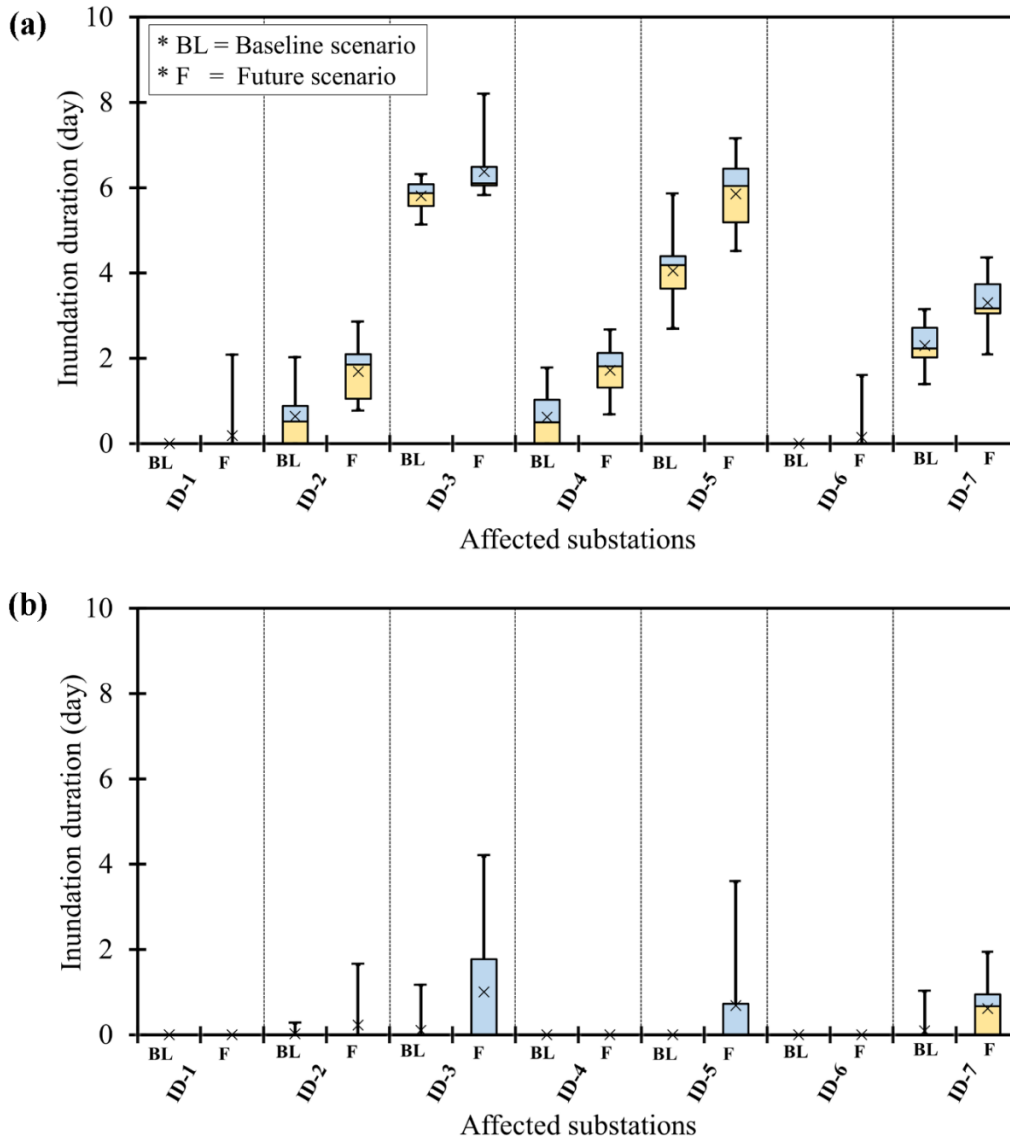
633 baseline period, while 7 substations are projected to be affected during the future period
634 (Figure 11a). Increases are indicated not only for the number of affected substations but
635 also for flood inundation depth values in the projected future climate. Overall, the mean
636 of the ensemble flood depth values shows an ~0.6 m increase in the future period (Figure
637 11a). Such an increase in the flood depth magnitude has the potential to exacerbate flood
638 related damage to electrical components, which can inflate the cost of hardening
639 measures such as elevating substations and constructing flood-protective barriers. As
640 expected, when the substations were flood-proofed up to BFE plus ~0.91 m (mitigation
641 scenario 2), the number of affected substations is reduced to three and four during the
642 baseline and future periods, respectively (Figure 11b). The locations of substations that
643 were impacted in the baseline period, in both mitigation scenarios, are consistent with the
644 Whitfield County Emergency Management Agency report map (EMA, 2016) that shows
645 the locations of critical facilities vulnerable to the historical flooding.

646 The maximum inundation durations at the affected substations are summarized in
647 Figure 12a (mitigation scenario 1) and Figure 12b (mitigation scenario 2). For both
648 mitigation scenarios and all affected substations, ensemble mean inundation durations
649 exhibited an increase under future climate condition. This increase in inundation duration
650 probably would render substations out of service for longer periods of time by making it
651 difficult to repair damaged substation equipment and restore grid services to customers.
652 The potential hazards and consequences may also extend to critical facilities that are
653 supplied by the affected substations. Similar to results presented in the previous sections,
654 these results demonstrate the need for improving existing flood mitigation measures by
655 incorporating the trends and uncertainties that originate from climate change. The

656 vulnerability analysis approach presented in this study will better equip floodplain
 657 managers to identify the most vulnerable substations and to recommend suitable
 658 adaptation measures, while allocating resources efficiently.



659
 660 Figure 11. A summary of maximum flood depths for substations that were affected in the
 661 baseline and/or future periods (a) without flood protection measures and (b) with flood
 662 protection measures. Note: Affected substations with their corresponding IDs are shown
 663 in Figure 1. There are no negative values in the vertical axis, as the minimum flood depth
 664 value is zero.



665

666 Figure 12. A summary of maximum inundation durations for substations that were
 667 affected in the baseline and/or future periods (a) without flood protection measures and
 668 (b) with flood protection measures. Note: Affected substations with their corresponding
 669 IDs are shown in Figure 1. There are no negative values in the vertical axis, as the
 670 minimum inundation duration is zero.

671

672 **4. Summary and Conclusion**

673 This paper applies an integrated modeling framework to evaluate climate change
674 impacts on flood regime, floodplain protection standards, and electricity infrastructures
675 across the Conasauga River Watershed in the southeastern United States. [Building on the](#)
676 [ensemble concept used by Gangrade et al. \(2019\) for PMF-scale inundation modeling](#)
677 [\(AEP < 10⁻⁴ %\), we focused on more frequent extreme streamflow events \(i.e., AEP](#)
678 [around 1–0.2%\) based on 11 downscaled CMIP5 GCMs in this study.](#) Our evaluation is
679 based on a climate-hydrologic-hydraulic modeling framework, which makes use of an
680 eleven member ensemble of downscaled climate simulations. Nine out of eleven
681 ensemble members project an increase in the flood inundation area in the future period.
682 Similarly, at the 1% AEP level, the flood inundation frequency curves indicate ~16 km²
683 increase in floodplain area under the future climate. The comparison between the flood
684 depth frequency maps from the baseline and future simulations indicated that, on average,
685 ~80% of grid cells exhibit a 0.2 to 1.5 m increase in the flood depth values. Without the
686 flood protection measures, of the 44 electric substations inside the watershed, 5 and 7
687 substations could be affected during the baseline and future periods, respectively. Even
688 after flood-proofing, three and four substations could still be affected in the baseline and
689 future periods. The increases in flood depth magnitude and inundation duration at the
690 affected substations in the future period will most likely damage more electrical
691 components, inflate the cost of hardening measures and render substations out of service
692 for a longer period of time.

693 Although future climate conditions are uncertain, our results demonstrate the needs
694 for (1) consideration of climate change in the floodplain management regulations; (2)

695 improvements in the conventional deterministic flood delineation approach through the
696 inclusion of probabilistic or ensemble-based methods, and (3) improvements in the
697 existing flood protection measures for critical electricity infrastructures through enhanced
698 hydro-meteorologic modeling capacities. In particular, rapidly advanced high-
699 performance computing capabilities have enabled the incorporation of computationally
700 intensive 2D hydraulics modeling in the ensemble-based hydroclimate impact
701 assessment. While the computational cost demonstrated in this study may still seem
702 steep, in the current speed of technology advancement, we will soon be able to implement
703 such a computationally intensive assessment for wide applications. The approach
704 presented in this study can be used by floodplain managers to develop flood depth
705 frequency maps and to identify the most vulnerable electric substations.

706 **Author Contribution**

707 *Dullo, Kalyanapu, Kao, Gangrade and Morales-Hernández* developed the concept for the
708 paper, designed the methodology and *Dullo* performed all the simulations required for the
709 study with feedback from all the co-authors. *Sharif, Ghafoor and Morales-Hernández*
710 focused on programming, software development and testing of existing code components.
711 *Ashfaq and Morales-Hernández* provided access to supercomputing machine hours on
712 ORNL's SUMMIT and RHEA computers. The manuscript was edited by *Dullo* with inputs
713 from the co-authors.

714 **Competing Interests**

715 The authors declare that they have no conflict of interest.

716 **Acknowledgments**

717 This study was supported by the US Air Force Numerical Weather Modeling
718 Program. TTD, MBS, AJK, and SG also acknowledge support by the Center of
719 Management, Utilization, and Protection of Water Resources at Tennessee Technological
720 University. Some portion of the project was funded by the UT Battelle Subcontract No:
721 4000164401. The research used resources of the Oak Ridge Leadership Computing
722 Facility at Oak Ridge National Laboratory. Some of the co-authors are employees of UT-
723 Battelle LLC under contract DE-AC05-00OR22725 with the US Department of Energy.
724 Accordingly, the US government retains and the publisher, by accepting the article for
725 publication, acknowledges that the US government retains a nonexclusive, paid-up,
726 irrevocable, worldwide license to publish or reproduce the published form of this
727 manuscript, or allow others to do so, for US government purposes. The input data sets are
728 cited throughout the paper, as appropriate.

729 **Data Availability**

730 The data that support the findings of this study are openly available in figshare
731 repository at the following URL:

732 https://figshare.com/projects/Conasauga_Flood_Modeling_Project/80840.

733 **References**

734 AECOM: The Impact of Climate Change and Population Growth on the National Flood
735 Insurance Program through 2100, available at: [https://www.aecom.com/content/wp-](https://www.aecom.com/content/wp-content/uploads/2016/06/Climate_Change_Report_AECOM_2013-06-11.pdf)
736 [content/uploads/2016/06/Climate_Change_Report_AECOM_2013-06-11.pdf](https://www.aecom.com/content/uploads/2016/06/Climate_Change_Report_AECOM_2013-06-11.pdf) (last
737 access: 12 October 2019), 2013.

738 Alfieri, L., Salamon, P., Bianchi, A., Neal, J., Bates, P., and Feyen, L.: Advances in Pan-
739 European Flood Hazard Mapping, *Hydrol. Process.*, 28(13), 4067–4077,
740 doi:10.1002/hyp.9947, 2014.

741 Alfieri, L., Burek, P., Feyen, L., and Forzieri, G.: Global Warming Increases the
742 Frequency of River Floods in Europe, *Hydrol. Earth Syst. Sci.*, 19, 2247–2260,
743 doi:10.5194/hess-19-2247-2015, 2015a.

744 Alfieri, L., Feyen, L., Dottori, F., and Bianchi, A.: Ensemble Flood Risk Assessment in
745 Europe Under High End Climate Scenarios, *Global Environ. Chang.*, 35, 199–212,
746 doi:10.1016/j.gloenvcha.2015.09.004, 2015b.

747 Alfieri, L., Bisselink, B., Dottori, F., Naumann, G., de Roo, A., Salamon, P., Wyser, K.,
748 and Feyen, L.: Global Projections of River Flood Risk in a Warmer World, *Earth’s*
749 *Future*, 5, 171–182, doi:10.1002/2016EF000485, 2017.

750 Alfieri, L., Dottori, F., Betts, R., Salamon, P., and Feyen, L.: Multi-Model Projections of
751 River Flood Risk in Europe under Global Warming, *Climate*, 6(6),
752 doi:10.3390/cli6010006, 2018.

753 Allen-Dumas, M. R., Binita, K. C., and Cunliff, C. I.: Extreme Weather and Climate
754 Vulnerabilities of the Electric Grid: A Summary of Environmental Sensitivity
755 Quantification Methods, ORNL/TM-2019/1252, Oak Ridge National Laboratory,
756 available at: [https://www.energy.gov/sites/prod/files/2019/09/f67/
757 Oak%20Ridge%20National%20Laboratory%20EIS%20Response.pdf](https://www.energy.gov/sites/prod/files/2019/09/f67/Oak%20Ridge%20National%20Laboratory%20EIS%20Response.pdf) (last access: 17
758 December 2019), 2019.

759 [Anderson, T. W., and Darling, D. A. Asymptotic theory of certain ‘goodness-of-fit’](#)
760 [criteria based on stochastic processes, Ann. Math, Stat., 23, 193-212, 1952. URL:](#)
761 <https://www.jstor.org/stable/2236446>

762 Archuleta, C.-A. M., Constance, E. W., Arundel, S. T., Lowe, A. J., Mantey, K. S., and
763 Phillips, L. A.: The National Map Seamless Digital Elevation Model Specifications,
764 US Geological Survey Techniques and Methods 11-B9, doi:10.3133/tm11B9,
765 available at: <https://pubs.er.usgs.gov/publication/tm11B9> (last access: 31 December
766 2019), 2017.

767 Arnell, N. W. and Gosling, S. N.: The Impacts of Climate Change on River Flood Risk at
768 the Global Scale, *Clim. Change*, 134, 387–401, doi:10.1007/s10584-014-1084-5,
769 2014.

770 Ashfaq, M., Bowling, L. C., Cherkauer, K., Pal, J. S., and Diffenbaugh, N. S.: Influence
771 of Climate Model Biases and Daily-scale Temperature and Precipitation Events on
772 Hydrological Impacts Assessment: A Case Study of the United States, *J. Geophys.*
773 *Res.*, 115, D14116, doi:10.1029/2009JD012965, 2010.

774 Ashfaq, M., Ghosh, S., Kao, S.-C., Bowling, L. C., Mote, P., Touma, D., Rauscher, S. A.,
775 and Diffenbaugh, N. S.: Near-term Acceleration of Hydroclimatic Change in the
776 Western U.S., *J. Geophys. Res.*, 118, 10,676–10, 693, doi:10.1002/jgrd.50816, 2013.

777 Ashfaq, M., Rastogi, D., Mei, R., Kao, S.-C., Gangrade, S., Naz, B. S., and Touma, D.:
778 High-resolution Ensemble Projections of Near-term Regional Climate over the
779 Continental United States. *J. Geophys. Res.*, 121, 9943–9963,
780 doi:10.1002/2016JD025285, 2016.

781 Baechler, M. C., Gilbride, T. L., Cole, P. C., Hefty, M. G., and Ruiz, K.: Building
782 America Best Practices Series, Volume 7.3, High-Performance Home Technologies:
783 Guide to Determining Climate Regions by County, Pacific Northwest National
784 Laboratory, US Department of Energy under Contract DE-AC05-76RLO 1830,
785 PNNL-17211 Rev. 3, available at:
786 https://www.energy.gov/sites/prod/files/2015/10/f27/ba_climate_region_guide_7.3.pdf
787 [f](#) (last access: 27 September 2020), 2015.

788 Bhuyian, Md. N. M., Kalyanapu, A. J., and Nardi, F.: Approach to Digital Elevation
789 Model Correction by Improving Channel Conveyance, *J. Hydrol. Eng.*, 20(5),
790 doi:10.1061/(ASCE)HE.1943-5584.0001020, 2014.

791 Bhuyian, Md. N. M., Dullo, T. T., Kalyanapu, A. J., Gangrade, S., and Kao, S.-C.:
792 Application of Geomorphic Correlations for River Bathymetry Correction in Two-
793 dimensional Hydrodynamic Modeling for Long-term Flood Risk Evaluation, World
794 Environmental and Water Resources Congress, Pittsburgh, Pennsylvania, USA, 19-23
795 May 2019, 2019.

796 Birhanu, D., Kim, H., Jang, C., and Park, S.: Flood Risk and Vulnerability of Addis
797 Ababa City Due to Climate Change and Urbanization, *Procedia Engineer.*, 154, 696–
798 702, doi:10.1016/j.proeng.2016.07.571, 2016.

799 Blessing, R., Sebastian, A., and Brody, S. D.: Flood Risk Delineation in the United
800 States: How Much Loss Are We Capturing?, *Nat. Hazards Rev.*, 18(3), 04017002-(1-
801 10), doi:10.1061/(ASCE)NH.1527-6996.0000242, 2017.

802 Bollinger, L. A. and Dijkema, G. P. J.: Evaluating Infrastructure Resilience to Extreme
803 Weather – the Case of the Dutch Electricity Transmission Network, *EJTIR*, 16(1),
804 214–239, doi:10.18757/ejtir.2016.16.1.3122, 2016.

805 Bragatto, T., Cresta, M., Cortesi, F., Gatta, F. M., Geri, A., Maccioni, M., and Paulucci,
806 M.: Assessment and Possible Solution to Increase Resilience: Flooding Threats in
807 Terni Distribution Grid, *Energies*, 12(4), 744, doi:10.3390/en12040744, 2019.

808 Brunner, G. W., Warner, J. C., Wolfe, B. C., Piper, S. S., and Marston, L.: Hydrologic
809 Engineering Center – River Analysis System (HEC-RAS) Applications Guide 2016,
810 Version 5.0, US Army Corps of Engineers, CA, available at:
811 <https://www.hec.usace.army.mil/software/hec-ras/documentation/HEC->
812 [RAS%205.0%20Applications%20Guide.pdf](https://www.hec.usace.army.mil/software/hec-ras/documentation/HEC-RAS%205.0%20Applications%20Guide.pdf) (last access: 27 December 2019), 2016.

813 Burkey, J.: Log-Pearson Flood Flow Frequency using USGS 17B, available at:
814 <https://www.mathworks.com/matlabcentral/fileexchange/22628-log-pearson-flood->
815 [flow-frequency-using-usgs-17b](https://www.mathworks.com/matlabcentral/fileexchange/22628-log-pearson-flood-flow-frequency-using-usgs-17b) (last access: 23 December 2019), 2009.

816 Chandramowli, S. N. and Felder, F. A.: Impact of Climate Change on Electricity Systems
817 and Markets – A Review of Models and Forecasts, *Sustain. Energy Technol. Assess.*,
818 5, 62–74, doi:10.1016/j.seta.2013.11.003, 2014.

819 Ciscar, J. C. and Dowling, P.: Integrated Assessment of Climate Impacts and Adaptation
820 in the Energy Sector, *Energy Econ.*, 46, 531–538, doi:10.1016/j.eneco.2014.07.003,
821 2014.

822 Cronin, J., Anandarajah, G., and Dessens, O.: Climate Change Impacts on the Energy
823 System: A Review of Trends and Gaps, *Clim. Change*, 151, 79–93,
824 doi:10.1007/s10584-018-2265-4, 2018.

825 Cook, A. and Merwade, V.: Effect of topographic data, geometric configuration and
826 modeling approach on flood inundation mapping, J. Hydrol., 377(1-2), 131-142,
827 doi:10.1016/j.jhydrol.2009.08.015, 2009.

828 Daly, C., Halbleib, M., Smith, J. I., Gibson, W. P., Doggett, M. K., Taylor, G. H., Curtis,
829 J., and Pasteris, P. P.: Physiographically Sensitive Mapping of Climatological
830 Temperature and Precipitation Across the Conterminous United States, Int. J.
831 Climatol., 28(15), 2031–2064, doi:10.1002/joc.1688, 2008.

832 Dey, S., Saksena, S., and Merwade, V.: Assessing the effect of different bathymetric
833 models on hydraulic simulation of rivers in data sparse regions, J. Hydrol., 575, 838-
834 851, doi:10.1016/j.jhydrol.2019.05.085, 2019.

835 Elliott, K. J. and Vose, J. M.: Initial Effects of Prescribed Fire on Quality of Soil Solution
836 and Streamwater in the Southern Appalachian Mountains, South. J. Appl. For., 29(1),
837 5–15, doi:10.1093/sjaf/29.1.5, 2005.

838 Elsner, M. M., Cuo, L., Voisin, N., Deems, J. S., Hamlet, A. F., Vano, J. A., Mickelson,
839 K. E. B., Lee, S.-Y., and Lettenmaier, D. P.: Implications of 21st Century Climate
840 Change for the Hydrology of Washington State, Climatic Change, 102(1–2), 225–
841 260, doi:10.1007/s10584-010-9855-0, 2010.

842 EMA (Emergency Management Agency): Whitfield County Hazard Mitigation Plan
843 2016, Including the Cities of Dalton, Tunnel Hill, and Varnell, and the Town of
844 Cohutta, Whitfield County Emergency Management Agency, available at:
845 <https://www.whitfieldcountyga.com/ema/WhitfieldHMPDraft52616.pdf> (last access:
846 29 March 2020), 2016.

847 England Jr., J. F., Cohn, T. A., Faber, B. A., Stedinger, J. R., Thomas Jr., W. O.,
848 Veilleux, A. G., Kiang, J. E., and Mason Jr., R. R.: Guidelines for Determining Flood
849 Flow Frequency—Bulletin 17C, Techniques and Methods 4-B5, US Geological
850 Survey, <https://doi.org/10.3133/tm4B5>, 2019.

851 Farber-DeAnda, M., Cleaver, M., Lewandowski, C., and Young, K.: Hardening and
852 Resiliency: US Energy Industry Response to Recent Hurricanes Seasons, Office of
853 Electricity Delivery and Energy Reliability, US Department of Energy, available at:
854 <https://www.oe.netl.doe.gov/docs/HR-Report-final-081710.pdf> (last access: 17
855 December 2019), 2010.

856 FEMA (Federal Emergency Management Agency): National Flood Insurance Program:
857 Program Description, Federal Emergency Management Agency, available at:
858 [https://www.fema.gov/media-library-data/20130726-1447-20490-
859 2156/nfipdescrip_1_.pdf](https://www.fema.gov/media-library-data/20130726-1447-20490-2156/nfipdescrip_1_.pdf) (last access: 22 January 2018), 2002.

860 FEMA (Federal Emergency Management Agency): Emergency Power Systems for
861 Critical Facilities: A Best Practices Approach to Improving Reliability, FEMA P-
862 1019, Applied Technology Council, Redwood City, CA, available at:
863 <https://www.fema.gov/media-library/assets/documents/101996> (last access: 17
864 December 2019), 2014.

865 FEMA (Federal Emergency Management Agency): FEMA Flood Map Service Center,
866 available at: <https://msc.fema.gov/portal/availabilitySearch?#searchresultsanchor>
867 (last access: 28 December 2019), 2019.

868 FIS (Flood Insurance Study): Flood Insurance Study: Whitfield County, Georgia and
869 Incorporated Areas, Flood Insurance Study Number: 13313CV000A, Federal

870 Emergency Management Agency, available at: <http://www.georgiadfirm.com/pdf/>
871 [panels/13313CV000A.pdf](http://www.georgiadfirm.com/pdf/panels/13313CV000A.pdf) (last access: 25 December 2019), 2007.

872 FIS (Flood Insurance Study): Flood Insurance Study: Murray County, Georgia and
873 Incorporated Areas, Flood Insurance Study Number: 13213CV000A, Federal
874 Emergency Management Agency, available at:
875 <http://www.georgiadfirm.com/pdf/panels/13213CV000A.pdf> (last access: 27
876 December 2019), 2010.

877 Forzieri, G., Bianchi, A., e Silva, F. B., Herrera, M. A. M., Leblois, A., Lavallo, C.,
878 Aerts, J. C. J. H., and Feyen, L.: Escalating Impacts of Climate Extremes on Critical
879 Infrastructures in Europe, *Glob. Environ. Change*, 48, 97–107,
880 doi:10.1016/j.gloenvcha.2017.11.007, 2018.

881 Fu, G., Wilkinson, S., Dawson, R. J., Fowler, H. J., Kilsby, C., Panteli, M., and
882 Mancarella, P.: Integrated Approach to Assess the Resilience of Future Electricity
883 Infrastructure Networks to Climate Hazards, *IEEE Syst. J.*, 12(4), 3169–3180,
884 doi:10.1109/JSYST.2017.2700791, 2017.

885 Galloway, G. E., Baecher, G. B., Plasencia, D., Coulton, K. G., Louthain, J., Bagha, M.,
886 and Levy, A. R.: Assessing the Adequacy of the National Flood Insurance Program’s
887 1 Percent Flood Standard, Water Policy Collaborative, University of Maryland,
888 available at: <https://www.fema.gov/media-library/assets/documents/9594> (last access:
889 17 December 2019), 2006.

890 Gangrade, S., Kao, S.-C., Naz, B. S., Rastogi, D., Ashfaq, M., Singh, N., and Preston, B.
891 L.: Sensitivity of Probable Maximum Flood in a Changing Environment, *Water*
892 *Resour. Res.*, 54(6), 3913–3936, doi:10.1029/2017WR021987, 2018.

893 Gangrade, S., Kao, S.-C., Dullo, T. T., Kalyanapu, A. J., and Preston, B. L.: Ensemble-
894 based Flood Vulnerability Assessment for Probable Maximum Flood in a Changing
895 Environment, *J. Hydrol.*, 576, 342–355, doi:10.1016/j.jhydrol.2019.06.027, 2019.

896 Gangrade, S., Kao, S.-C., and McManamay, R. A.: Multi-model Hydroclimate
897 Projections for the Alabama-Coosa-Tallapoosa River Basin in the Southeastern
898 United States, *Sci. Rep.*, 10, 2870, doi:10.1038/s41598-020-59806-6, 2020.

899 Gilstrap, M., Amin, S., and DeCorla-Souza, K.: United States Electricity Industry Primer,
900 DOE/OE-0017, Office of Electricity Delivery and Energy Reliability, US Department
901 of Energy, Washington DC, available at:
902 [https://www.energy.gov/sites/prod/files/2015/12/f28/united-states-electricity-
903 industry-primer.pdf](https://www.energy.gov/sites/prod/files/2015/12/f28/united-states-electricity-
903 industry-primer.pdf) (last access: 17 December 2019), 2015.

904 Giorgi, F., Coppola, E., Solmon, F., Mariotti, L., Sylla, M. B., Bi, X., Elguindi, N., Diro,
905 G. T., Nair, V., Giuliani, G., Turuncoglu, U. U., Cozzini, S., Güttler, I., O’Brien, T.
906 A., Tawfik, A. B., Shalaby, A., Zakey, A. S., Steiner, A. L., Stordal, F., Sloan, L. C.,
907 and Brankovic, C.: RegCM4: model description and preliminary tests over multiple
908 CORDEX domains, *Climate Res.*, 52, 7–29, doi:10.3354/cr01018, 2012.

909 HCFCD (Harris County Flood Control District): Hurricane Harvey – Storm and Flood
910 Information, available at: [https://www.hcfc.org/Portals/62/Harvey/immediate-flood-
911 report-final-hurricane-harvey-2017.pdf](https://www.hcfc.org/Portals/62/Harvey/immediate-flood-
911 report-final-hurricane-harvey-2017.pdf) (last access: 16 December 2019), 2018.

912 HIFLD (Homeland Infrastructure Foundation-Level Data): Homeland Infrastructure
913 Foundation-Level Data, Electric Substations, US Department of Homeland Security,
914 available at: [https://hifld-geoplatform.opendata.arcgis.com/datasets/electric-
915 substations](https://hifld-geoplatform.opendata.arcgis.com/datasets/electric-
915 substations) (last access: 20 December 2019), 2019.

916 Hirabayashi, Y., Mahendran, R., Koirala, S., Konoshima, L., Yamazaki, D., Watanabe,
917 S., Kim, H., and Kanae, S.: Global Flood Risk under Climate Change, *Nature Clim.*
918 *Chang.*, 3, 816–821, doi:10.1038/NCLIMATE1911, 2013.

919 Hou, Z., Ren, H., Sun, N., Wigmosta, M. S., Liu, Y., Leung, L. R., Yan, H., Skaggs, R.,
920 and Coleman, A.: Incorporating Climate Nonstationarity and Snowmelt Processes in
921 Intensity–Duration–Frequency Analyses with Case Studies in Mountainous Areas, *J.*
922 *Hydrometeorol.*, 20(12), 2331–2346, doi:10.1175/JHM-D-19-0055.1, 2019.

923 Ivey, G. and Evans, K.: Conasauga River Alliance Business Plan: Conasauga River
924 Watershed Ecosystem Project, available at: [https://www.fs.fed.us/
925 \[largewatershedprojects/businessplans/\]\(https://www.fs.fed.us/largewatershedprojects/businessplans/\)](https://www.fs.fed.us/largewatershedprojects/businessplans/) (last access: 22 December 2019), 2000.

926 [Kalyanapu, A. J., Burian, S. J., and McPherson, T. N.: Effect of Land Use-Based Surface](#)
927 [Roughness on Hydrologic Model Output, *Journal of Spatial Hydrology*, 9\(2\), 51–71,](#)
928 [2009.](#)

929 Kalyanapu, A. J., Shankar, S., Pardyjak, E. R., Judi, D. R., and Burian, S. J.: Assessment
930 of GPU Computational Enhancement to a 2D Flood Model, *Environ. Modell. Softw.*,
931 26(8), 1009–1016, doi:10.1016/j.envsoft.2011.02.014, 2011.

932 Kefi, M., Mishra, B. K., Kumar, P., Masago, Y., and Fukushi, K.: Assessment of
933 Tangible Direct Flood Damage Using a Spatial Analysis Approach under the Effects
934 of Climate Change: Case Study in an Urban Watershed in Hanoi, Vietnam, *Int. J.*
935 *Geo-Inf.*, 7, 29, doi:10.3390/ijgi7010029, 2018.

936 Kollat, J. B., Kasprzyk, J. R., Thomas Jr., W. O., Miller, A. C., and Divoky, D.:
937 Estimating the Impacts of Climate Change and Population Growth on Flood

938 Discharges in the United States, *J. Water Resour. Plann. Manage.*, 138(5), 442–452,
939 doi:10.1061/(ASCE)WR.1943-5452.0000233, 2012.

940 Langerwisch, F., Rost, S., Gerten, D., Poulter, B., Rammig, A., and Cramer, W.: Potential
941 Effects of Climate Change on Inundation Patterns in the Amazon Basin, *Hydrol.*
942 *Earth Syst. Sci.*, 17, 2247–2262, doi:10.5194/hess-17-2247-2013, 2013.

943 Li, H., Sun, J., Zhang, H., Zhang, J., Jung, K., Kim, J., Xuan, Y., Wang, X., and Li, F.:
944 What Large Sample Size Is Sufficient for Hydrologic Frequency Analysis? – A
945 Rational Argument for a 30-Year Hydrologic Sample Size in Water Resources
946 Management, *Water*, 10, 430, doi:10.3390/w10040430, 2018.

947 Marshall, R., Ghafoor, S., Rogers, M., Kalyanapu, A., and Dullo, T. T.: Performance
948 Evaluation and Enhancements of a Flood Simulator Application for Heterogeneous
949 HPC Environments, *Int. J. Network Comput.*, 8(2), 387–407, 2018.

950 McCuen, R. H.: *Hydrologic Analysis and Design, Third Edition, Pearson-Prentice Hall,*
951 *Upper Saddle River, New Jersey, 2005.*

952 Mikellidou, C. V., Shakou, L. M., Boustras, G., and Dimopoulos, C.: Energy Critical
953 Infrastructures at Risk from Climate Change: A State of the Art Review, *Saf. Sci.*,
954 110, 110–120, doi:10.1016/j.ssci.2017.12.022, 2018.

955 Milly, P. C. D., Wetherald, R. T., Dunne, K. A., and Delworth, T. L.: Increasing Risk of
956 Great Floods in a Changing Climate, *Nature*, 415(6871), 514–517,
957 doi:10.1038/415514a, 2002.

958 Mora, C., Spirandelli, D., Franklin, E. C., Lynham, J., Kantar, M. B., Miles, W., Smith,
959 C. Z., Freel, K., Moy, J., Louis, L. V., Barba, E. W., Bettinger, K., Frazier, A. G.,
960 Colburn IX, J. F., Hanasaki, N., Hawkins, E., Hirabayashi, Y., Knorr, W., Little, C.

961 M., Emanuel, K., Sheffield, J., Patz, J. A., and Hunter, C. L.: Broad Threat to
962 Humanity from Cumulative Climate Hazards Intensified by Greenhouse Gas
963 Emissions, *Nature Clim. Chang.*, 8, 1062–1071, doi:10.1038/s41558-018-0315-6,
964 2018.

965 Morales-Hernández, M., Sharif, M. B., Gangrade, S., Dullo, T. T., Kao, S.-C.,
966 Kalyanapu, A., Ghafoor, S. K., Evans, K. J., Madadi-Kandjani, E., and Hodges, B. R.:
967 High Performance Computing in Water Resources Hydrodynamics, *Journal of*
968 *Hydroinformatics*, in press, ~~2020a~~2020.

969 Morales-Hernández, M., Sharif, Md. B., Kalyanapu, A., Ghafoor, S. K., Dullo, T.T.,
970 Gangrade, S., Kao, S.-C., Norman, M. R., and Evans, K. J.: TRITON: A Multi-GPU
971 Open Source 2D Hydrodynamic Flood, ~~Submitted to~~ *Environmental Modelling &*
972 *Software*, in press, 2020b2021.

973 MRLC (Multi-Resolution Land Characteristics Consortium): National Land Cover
974 Database (NLCD), available at: [https://www.mrlc.gov/data/nlcd-2011-land-cover-](https://www.mrlc.gov/data/nlcd-2011-land-cover-conus-0)
975 [conus-0](https://www.mrlc.gov/data/nlcd-2011-land-cover-conus-0) (last access: 5 May 2020), 2011.

976 NERC (North American Electric Reliability Corporation): Hurricane Harvey Event
977 Analysis Report, North American Electric Reliability Corporation, Atlanta, GA,
978 available at: [https://www.nerc.com/pa/rrm/ea/Hurricane_Harvey_EAR_DL/](https://www.nerc.com/pa/rrm/ea/Hurricane_Harvey_EAR_DL/NERC_Hurricane_Harvey_EAR_20180309.pdf)
979 [NERC Hurricane Harvey EAR 20180309.pdf](https://www.nerc.com/pa/rrm/ea/Hurricane_Harvey_EAR_20180309.pdf) (last access: 17 December 2019),
980 2018.

981 Ntelekos, A. A., Oppenheimer, M., Smith, J. A., and Miller, A. J.: Urbanization, Climate
982 Change and Flood Policy in the United States, *Clim. Chang.*, 103, 597–616,
983 doi:10.1007/s10584-009-9789-6, 2010.

984 Nyaupane, N., Thakur, B., Kalra, A., and Ahmad, S.: Evaluating Future Flood Scenarios
985 Using CMIP5 Climate Projections, *Water*, 10, 1866, doi:10.3390/w10121866, 2018.

986 Olsen, J. R.: Climate Change and Floodplain Management in the United States, *Clim.*
987 *Change*, 76, 407–426, doi:10.1007/s10584-005-9020-3, 2006.

988 Pachauri, R. K. and Meyer, L. A.: Intergovernmental Panel on Climate Change (IPCC):
989 Climate Change 2014: Synthesis Report, in Proceedings of Contribution of Working
990 Groups I, II and III to the Fifth Assessment Report of the Intergovernmental Panel on
991 Climate Change, Geneva, Switzerland, available at:
992 https://www.ipcc.ch/site/assets/uploads/2018/05/SYR_AR5_FINAL_full_wcover.pdf
993 (last access: 16 December 2019), 2014.

994 Pant, R., Thacker, S., Hall, J. W., Alderson, D., and Barr, S.: Critical Infrastructure
995 Impact Assessment Due to Flood Exposure, *J. Flood Risk Manag.*, 11, 22–33,
996 doi:10.1111/jfr3.12288, 2017.

997 Pielke Jr., R. A. and Downton, M. W.: Precipitation and Damaging Floods: Trends in the
998 United States, 1932–97, *J. Climate*, 13(20), 3625–3637, doi:10.1175/1520-
999 0442(2000)013<3625:PADFTI>2.0.CO;2, 2000.

1000 Pielke Jr., R. A., Downton, M. W., and Barnard Miller, J. Z.: Flood Damage in the United
1001 States, 1926–2000: A reanalysis of National Weather Service Estimates, National
1002 Center for Atmospheric Research, Boulder, CO, available at:
1003 <https://sciencepolicy.colorado.edu/flooddamagedata/flooddamagedata.pdf> (last
1004 access: 16 December 2019), 2002.

1005 Pralle, S.: Drawing Lines: FEMA and the Politics of Mapping Flood Zones, *Clim.*
1006 *Chang.*, 152, 227–237, doi:10.1007/s10584-018-2287-y, 2019.

1007 Reed, D. A., Kapur, K. C., and Christie, R. D.: Methodology for Assessing the Resilience
1008 of Networked Infrastructure, *IEEE Syst. J.*, 3(2), 174–180,
1009 doi:10.1109/JSYST.2009.2017396, 2009.

1010 Saksena, S., Dey, S., Merwade, V., & Singhofen, P. J. (2020). A computationally
1011 efficient and physically based approach for urban flood modeling using a flexible
1012 spatiotemporal structure. *Water Resources Research*, 56, e2019WR025769.
1013 <https://doi.org/10.1029/2019WR025769>

1014 Storck, P., Bowling, L., Wetherbee, P., and Lettenmaier, D.: Application of a GIS-Based
1015 Distributed Hydrology Model for Prediction of Forest Harvest Effects on Peak
1016 Stream Flow in the Pacific Northwest, *Hydrol. Process.*, 12(6), 889–904,
1017 doi:10.1002/(SICI)1099-1085(199805)12:6<889::AID-HYP661>3.0.CO;2-P, 1998.

1018 Strauss, B. and Ziemiński, R.: Sea Level Rise Threats to Energy Infrastructure: A
1019 Surging Seas Brief Report by Climate Central, Climate Central, Washington, DC,
1020 available at: <http://slr.s3.amazonaws.com/SLR-Threats-to-Energy-Infrastructure.pdf>
1021 (last access: 17 December 2019), 2012.

1022 Tan, A.: Sandy and Its Impacts: Chapter 1, NYC Special Initiative for Rebuilding and
1023 Resiliency, NYC Resources, NY, available at:
1024 [http://www.nyc.gov/html/sirr/downloads/pdf/final_report/Ch_1_SandyImpacts_FINAL](http://www.nyc.gov/html/sirr/downloads/pdf/final_report/Ch_1_SandyImpacts_FINAL_singles.pdf)
1025 [L_singles.pdf](http://www.nyc.gov/html/sirr/downloads/pdf/final_report/Ch_1_SandyImpacts_FINAL_singles.pdf) (last access: 17 December 2019), 2013.

1026 Thornton, P. E., Running, S. W., and White, M. A.: Generating surfaces of daily
1027 meteorological variables over large regions of complex terrain, *J. Hydrol.*, 190, 214–
1028 251, doi:10.1016/S0022-1694(96)03128-9, 1997.

1029 UNISDR (United Nations Office for Disaster Risk Reduction): Making Development
1030 Sustainable: The Future of Disaster Risk Management, Global Assessment Report on
1031 Disaster Risk Reduction, Geneva, Switzerland, available at:
1032 [https://www.preventionweb.net/english/hyogo/gar/2015/en/gar-](https://www.preventionweb.net/english/hyogo/gar/2015/en/gar-pdf/GAR2015_EN.pdf)
1033 [pdf/GAR2015_EN.pdf](https://www.preventionweb.net/english/hyogo/gar/2015/en/gar-pdf/GAR2015_EN.pdf) (last access: 16 December 2019), 2015.

1034 USACE (US Army Corps of Engineers): Master Water Control Manual: Alabama-Coosa-
1035 Tallapoosa (ACT) River Basin, Alabama, Georgia, US Army Corps of Engineers,
1036 available at: [https://www.sam.usace.army.mil/Portals/46/docs/](https://www.sam.usace.army.mil/Portals/46/docs/planning_environmental/act/docs/New/ACT%20Master%20Manual_March%202013.pdf)
1037 [planning_environmental/act/docs/New/ACT%20Master%20Manual_March%202013.pd](https://www.sam.usace.army.mil/Portals/46/docs/planning_environmental/act/docs/New/ACT%20Master%20Manual_March%202013.pdf)
1038 [f](https://www.sam.usace.army.mil/Portals/46/docs/planning_environmental/act/docs/New/ACT%20Master%20Manual_March%202013.pdf) (last access: 22 December 2019), 2013.

1039 USGS (US Geological Survey): Guidelines for Determining Flood Flow Frequency,
1040 Bulletin #17B of the Hydrology Subcommittee, Interagency Advisory Committee on
1041 Water Data, US Geological Survey, Reston, VA, 1982.

1042 Vale, M.: Securing the US Electrical Grid, Center for the Study of the Presidency and
1043 Congress (CSPC), Washington DC, available at: [https://protectourpower.org/](https://protectourpower.org/resources/cspc-2014.pdf)
1044 [resources/cspc-2014.pdf](https://protectourpower.org/resources/cspc-2014.pdf) (last access: 14 March 2017), 2014.

1045 Wigmosta, M. S., Vail, L. W., and Lettenmaier, D. P.: A Distributed Hydrology-
1046 Vegetation Model for Complex Terrain, *Water Resour. Res.*, 30(6), 1665–1679,
1047 doi:10.1029/94WR00436, 1994.

1048 Wigmosta, M. S., Nijssen, B., Storck, P., and Lettenmaier, D. P.: The Distributed
1049 Hydrology Soil Vegetation Model, in *Mathematical Models of Small Watershed*
1050 *Hydrology and Applications*, V. P. Singh, D. K. Frevert, eds., *Wat. Resour.*
1051 *Publications*, Littleton, CO, 2002.

1052 Wilbanks, T. J., Bhatt, V., Bilello, D., Bull, S., Ekmann, J., Horak, W., Huang, Y. J.,
1053 Levine, M. D., Sale, M. J., Schmalzer, D., and Scott, M. J.: Effects of Climate
1054 Change on Energy Production and Use in the United States, US Climate Change
1055 Science Program Synthesis and Assessment Product 4.5, available at:
1056 <https://digitalcommons.unl.edu/cgi/viewcontent.cgi?article=1005&context=usdoepub>
1057 (last access: 17 December 2019), 2008.

1058 Wing, O. E. J., Bates, P. D., Sampson, C. C., Smith, A. M., Johnson, K. A., and Erickson,
1059 T. A.: Validation of a 30 m Resolution Flood Hazard Model of the Conterminous
1060 United States, *Water Resour. Res.*, 53, 7968–7986, doi:10.1002/2017WR020917,
1061 2017.

1062 Wing, O. E. J., Bates, P. D., Smith, A. M., Sampson, C. C., Johnson, K. A., Fargione, J.,
1063 and Morefield, P.: Estimates of Present and Future Flood Risk in the Conterminous
1064 United States, *Environ. Res. Lett.*, 13(3), 034023, doi:10.1088/1748-9326/aaac65,
1065 2018.

1066 Winkler, J., Duenas-Osorio, L., Stein, R., and Subramanian, D.: Performance Assessment
1067 of Topologically Diverse Power Systems Subjected to Hurricane Events, *Reliability*
1068 *Engineering and System Safety*, 95(4), 323–336, doi:10.1016/j.res.2009.11.002,
1069 2010.

1070 Winsemius, H. C., Aerts, J. C. J. H., van Beek, L. P. H., Bierkens, M. F. P., Bouwman,
1071 A., Jongman, B., Kwadijk, J. C. J., Ligtoet, W., Lucas, P. L., van Vuuren, D. P., and
1072 Ward, P. J.: Global Drivers of Future River Flood Risk, *Nat. Clim. Chang.*, 6, 381–
1073 385, doi:10.1038/NCLIMATE2893, 2016.

1074 Wobus, C., Gutmann, E., Jones, R., Rissing, M., Mizukami, N., Lorie, M., Mahoney, H.,
1075 Wood, A. W., Mills, D., and Martinich, J.: Climate Change Impacts on Flood Risk
1076 and Asset Damages within Mapped 100-year Floodplains of the Contiguous United
1077 States, *Nat. Hazards Earth Syst. Sci.*, 17, 2199–2211, doi:10.5194/nhess-17-2199-
1078 2017, 2017.

1079 Zamuda, C., Antes, M., Gillespie, C. W., Mosby, A., and Zotter, B.: Climate Change and
1080 the US Energy Sector: Regional Vulnerabilities and Resilience Solutions, Office of
1081 Energy Policy and Systems Analysis, US Department of Energy, available at:
1082 [https://energy.gov/sites/prod/files/2015/10/f27/Regional_Climate_Vulnerabilities_and](https://energy.gov/sites/prod/files/2015/10/f27/Regional_Climate_Vulnerabilities_and_Resilience_Solutions_0.pdf)
1083 [Resilience_Solutions_0.pdf](https://energy.gov/sites/prod/files/2015/10/f27/Regional_Climate_Vulnerabilities_and_Resilience_Solutions_0.pdf) (last access: 17 December 2019), 2015.

1084 Zamuda, C. and Lippert, A.: Climate Change and the Electricity Sector: Guide for
1085 Assessing Vulnerabilities and Developing Resilience Solutions to Sea Level Rise,
1086 Office of Energy Policy and Systems Analysis, US Department of Energy, available
1087 at: [https://toolkit.climate.gov/sites/default/files/Climate%20Change%20](https://toolkit.climate.gov/sites/default/files/Climate%20Change%20and%20the%20Electricity%20Sector%20Guide%20for%20Assessing%20Vulnerabilities%20and%20Developing%20Resilience%20Solutions%20to%20Sea%20Level%20Rise%20July%202016.pdf)
1088 [and%20the%20Electricity%20Sector%20Guide%20for%20Assessing%20Vulnerabili](https://toolkit.climate.gov/sites/default/files/Climate%20Change%20and%20the%20Electricity%20Sector%20Guide%20for%20Assessing%20Vulnerabilities%20and%20Developing%20Resilience%20Solutions%20to%20Sea%20Level%20Rise%20July%202016.pdf)
1089 [ties%20and%20Developing%20Resilience%20Solutions%20to%20Sea%20Level%2](https://toolkit.climate.gov/sites/default/files/Climate%20Change%20and%20the%20Electricity%20Sector%20Guide%20for%20Assessing%20Vulnerabilities%20and%20Developing%20Resilience%20Solutions%20to%20Sea%20Level%20Rise%20July%202016.pdf)
1090 [ORise%20July%202016.pdf](https://toolkit.climate.gov/sites/default/files/Climate%20Change%20and%20the%20Electricity%20Sector%20Guide%20for%20Assessing%20Vulnerabilities%20and%20Developing%20Resilience%20Solutions%20to%20Sea%20Level%20Rise%20July%202016.pdf) (last access: 18 December 2019), 2016.

1091 Zhao, G., Gao, H., Naz, B. S., Kao, S.-C., and Voisin, N.: Integrating a Reservoir
1092 Regulation Scheme into a Spatially Distributed Hydrological Model, *Adv. Water*
1093 *Resour.*, 98, 16–31, doi:10.1016/j.advwatres.2016.10.014, 2016.

1094 Zheng, X., Maidment, D. R., Tarboton, D. G., Liu, Y. Y., and Passalacqua, P.: GeoFlood:
1095 Large-scale Flood Inundation Mapping Based on High-Resolution Terrain Analysis,
1096 *Water Resour. Res.*, 54, 10,013–10,033, doi:10.1029/2018WR023457, 2018.